Hindawi
International Transactions on Electrical Energy Systems
Volume 2022, Article ID 5440326, 23 pages
https://doi.org/10.1155/2022/5440326

Research Article

Chaos and Dynamics Induced by the Amplitude of Load Torque: Analysis and Control

Arnaud Ngonting Topy,[1,2] Justin Roger Mboupda Pone,[1,2] Alex Stephane Kemnang Tsafack,[2] and Romanic Kengne[2]

[1]*Research Unit of Automation and Applied Computer (UR-AIA), Electrical Engineering Department of IUT-FV, University of Dschang, P.O. Box: 134, Bandjoun, Cameroon*
[2]*Research Unit of Condensed Matter of Electronics and Signal Processing. Department of Physics, Faculty of Sciences, University of Dschang, P.O. Box 67, Dschang, Cameroon*

Correspondence should be addressed to Justin Roger Mboupda Pone; pone00@yahoo.com

Received 31 December 2021; Revised 29 March 2022; Accepted 3 June 2022; Published 30 June 2022

Academic Editor: Gulshan Sharma

In this contribution, the dynamics and chaos control of a permanent magnet reluctance synchronous motor (PMSM) with constant, sinusoidal, and square load torque taking the reference rotor speed and the stator voltage on d-q-axis are analyzed. The analysis shows that under some conditions, varying amplitude of the load torque, PMSM presents period doubling route to chaos with one and double-scroll attractors and bursting oscillations. We use the self-feedback delay controller to stabilize the output trajectory by forcing to the periodic solution. Furthermore, an analog circuit is designed and implemented in OrCAD-PSpice software to verify the numerical results and good agreement is observed with numerical results.

1. Introduction

Many industries use the permanent magnet reluctance synchronous motor (PMSM) as the most reliable actuator. PMSM is a type of synchronous reluctance motor which overcomes problems such as torque pulsation, fault tolerance, and acoustic noises [1]. The PMSM offers high-performance drive when uses torques due the magnets and reluctance variation; note that the machine has a problem of high speed [2]. The dynamics characteristics, speed control, and oscillations of different types of motor and generator are studies since references [3–9]. Recently, literature works have been focused on non-nonlinear phenomena arising in PMSM electrical machine [10–13]. The bifurcation and chaos in PMSM use a simplifier model of the motor by neglecting/eliminating some parameters, demonstrated that the system could exhibit different dynamic characteristics, such as limit circle, steady state, and chaos [14]. The study of synchronous motor with load vibration shows that with constant and sinusoidal load torque, synchronous motor exhibits chaotic phenomena [15–17]. The investigation of dynamical behaviors and the control of chaos in indirect field-oriented control (IFOC) of 3-phases and implementation of the self-feedback delay controller are studies [18, 19]. The bifurcation and chaos theory are used to study stability of the PMSM as a nonlinear system [20–22]. Hemati and Leu in [23, 24] present the permanent-magnet machines dynamics and investigate the steady-state characteristics of the machine, driving a constant load torque with the constant input voltages. They show that the permanent-magnet machines under investigation have multiple equilibria which deeply influence the general stability of machine [25]. The authors in [26] chose the estimation error of rotor time constant as bifurcation parameter in the IFOC, and they show that chaos and limit cycles arise for some ranges of load torque with certain PI speed controller setting. The authors in [26] show the effect of the estimation error of rotor time constant taking as a bifurcation parameter in the IFOC, and they show that the motor exhibits chaos and periodic behaviors for some ranges of load torque with certain

proportional integral speed controller parameter. The paper [27] used the numerical study to understand the dynamic behavior of IFOC of a current-fed induction motor, and they discussed different forms of transition to chaos in the motor model. By analysing the bifurcation results, the authors provide important information for modifying both the motor model and the proportional integral controller settings. In state variable participation in the limit cycle of IM (induction motor), they showed that the dynamics of a single-phase capacitor-operated motor can be determined by the profile of several state variables [28]. The IFOC of 3-phase induction motor enters chaotic state by period doubling route phenomena after Hopf bifurcation. In [17], the dynamical analysis and control of chaos in the permanent magnet synchronous reluctance motor (SynRM) are shown with two types of load torque: constant and sinusoidal. In this work, the authors considered a motor with lord vibration perturbation and the system exhibits, pitchfork bifurcation, double-scroll chaotic attractor, and multistability. However, during the study, the authors focused only on the influence of the frequency (parameter of study) of the load on the dynamics of the SynRM, neglecting the effects of the variation of the amplitude of each load torque whereas this parameter is very important to take into account.

In fact, in industries, the PMSM is aim to drive different loads during its operation. In this contribution, we highlighted the industrial situations where the amplitude of the load torque is varied in contrast to constant and frequency variation presented in the literature. In addition, the approach where the load torque is on and off depending on the process driven by the PMSM is also studied. We found some striking dynamics not yet observed here and therefore highlighted some engineering malfunctioning not yet explained.

Motivated by the above shortcomings, the rich results obtained in the previous work published in good standing papers and the importance of PMSM in industries applications, we focused on the key idea of this work that is the discussion of some results regarding the investigation of the dynamic behavior of PMSM where some new phenomena take place from the best of our knowledge under the variation of the amplitude of different load torque (constant, sinusoidal, and square). On the above discussions, the main objective in this work is the analytical studies of the dynamic of PMSM with

(i) constant load torque

(ii) amplitude of the sinusoidal load torque

(iii) amplitude square load torque

At the end of the paper, the time delay control to suppress the chaotic behavior in this type of machine is presented.

The rest of the paper is organised as follows: Section 2 presents the mathematical model of the PMSM derived from good standing papers. Section 3 displays the analytical investigations, and we present the dynamical results obtained by varying the amplitude of different types of load torque in Section 4. The analog circuit verifications are shown in Section 5. Section 6 shows the control of the chaos in the system and then follows a conclusion in Section 7.

2. The Model of the Permanent Magnet Reluctance Synchronous Motor with Load Vibration Perturbation

The electrical dynamical system of PMSM uses in this work is described by [29] and recall here as in the following equations:

$$\frac{di_q}{dt} = \frac{\left(-Ri_q - nL_d\omega i_d - nk_t\omega + v_q\right)}{L_q}, \tag{1a}$$

$$\frac{di_d}{dt} = \frac{\left(-Ri_d + nL_q\omega i_q + v_d\right)}{L_d}. \tag{1b}$$

$j\dot{\omega} = T(I,\theta) - T_i(t)$. The equation describing the electromagnetic torque is given by

$$T\left(i_q, i_d\right) = n\left(k_t i_q + \left(L_d - L_q\right) i_q i_d\right) L_d, \tag{2}$$

where $k_t = \sqrt{(3/2)k_e}$, i_q, i_d are d- and q-axis rotor currents, ω is the mechanical rotor speed, and v_d and v_q are the stator voltage on d-q-axis. L_d and L_q are the d- and q-axis stator inductor, respectively, the stator winding resistance is R, and the polar moment of inertia is j. n is the number of pole-pairs $T(I,\theta)$ is the torque generated by the motor, and $T_1(t)$ represents the external torque applied to the motor shaft, including viscous and friction, given by $T_1 = b\omega + T_L$ where b is the viscous friction coefficient and T_L account for external load torque applied on the system. More details on modeling of PMSM can be found in [30]. After some transformations in [24], by using the affine transformation $x = \lambda\tilde{x}$ and the time-scaling transformation $t = \lambda\tilde{t}$ where $x = [\, iq \;\; id \;\; \omega \,]$, $\tilde{x} = [\, \tilde{i}q \;\; \tilde{i}d \;\; \tilde{\omega} \,]$ and $\tau = Lq/R$, we obtain the system equations of PMSM machine that take the following form:

$$\frac{d\tilde{i}q}{dt} = \tilde{v}_q - \tilde{i}q - \tilde{i}d\tilde{\omega} + c\tilde{\omega}, \tag{3a}$$

$$\frac{d\tilde{i}d}{dt} = \tilde{v}_d - \tilde{i}d + \tilde{i}q\tilde{\omega}, \tag{3b}$$

$$\frac{d\tilde{\omega}}{dt} = \sigma\left(\tilde{i}q - \tilde{\omega}\right) + \varepsilon\tilde{i}d\tilde{i}q - \tilde{T}_L, \tag{3c}$$

where $c = -(kt/kLq)$, $\sigma = b\tau/J$, $\tilde{v}\;\; q = (1/Rk)vq$, $\tilde{v}d = (1/Rk)vd$, $k = b/n\tau kt$, $\beta = R/Ld$, $\varepsilon = (nb\tau^2k^2(Ld - Lq))/J$, and $\tilde{T}_L = (\tau^2/J)T_L$ by introducing the transformation $x = \tilde{i}_q$, $y = \tilde{i}_d$, $z = \tilde{\omega}$, $T_3 = \tilde{T}_L$, $v = \tilde{u}_d$, and $u = \tilde{u}_q$ (3c).

The dimensionless form of the mathematical model of the machine is described as follows:

$$\frac{dx}{dt} = u - x - yz + cz, \tag{4a}$$

$$\frac{dy}{dt} = v - \beta y + xz, \tag{4b}$$

$$\frac{dz}{dt} = \sigma(x - z) - T_3, \tag{4c}$$

where z, y, x denote angle speed, quadrature- and direct-axis current of the motor, respectively. T_3 is the load torque. The system parameters c, β, σ are determined by the type of PMSM. We are considering that the reference rotor speed and the stator voltage on d-q-axis are not equal to zero ($u \neq 0$, $T_3 \neq 0$, $v \neq 0$). To study the dynamical behavior of the system of equations 4a–4c under load vibration perturbation, it is good to consider around three cases: (i) a constant torque load is applied to the PMSM, (ii) a sinusoidal load torque, and finally (iii) the square load torque is applied to the PMSM.

3. Analytical Studies

3.1. Dissipative Property. The contraction rate of system (4a–4c) is an easy way to check the possibility to develop the attractor [31]. By evaluating the contraction rate of system (4a–4c), it is as follows:

$$\Delta V = \frac{\partial(dx/dt)}{\partial x} + \frac{\partial(dy/dt)}{\partial y} + \frac{\partial(dz/dt)}{\partial z} = -(\beta + \sigma + 1). \tag{5}$$

We choose $\beta + \sigma \geq 0$; therefore, $-(\beta + \sigma + 1) < 0$ system (4a–4c) is dissipative and can develop attractors.

3.2. Equilibrium Points and Stability Studies. The equilibrium point is the foundation of the stability behavior of dynamical systems [32], because their study provides preliminary knowledge on the dynamics of the system. This is deduced by setting the derivatives in system (4a–4c) equal to zero; hence, $dx/dt = 0$, $dy/dt = 0$, $dz/dt = 0$. Obviously, the origin of the state space is a trivial equilibrium point. The other nonzero equilibrium points can be solved by the following equations, which gives

$$x_0 = \frac{T_3}{\sigma} + z_0, \tag{6a}$$

$$y_0 = \frac{1}{\beta}\left(\frac{T_3}{\sigma} z_0 + z_0 + v\right), \tag{6b}$$

$$-\frac{1}{\beta} z_0 - \frac{T_3}{\beta\sigma} z_0^2 + z_0\left(c - \frac{v}{\beta} - 1\right) + u - \frac{T_3}{\sigma} = 0. \tag{6c}$$

After some algebraic manipulations, equation (6c) becomes a transcendental equation with the parameters (β, σ, c). In this situation, it is easy to plot equation (6c) with the parameter T_3 in a discrete interval to raise the equilibrium points (see Figure 1).

The Jacobian matrix at any equilibrium point $E(x_0, y_0, z_0)$ is given as the follows:

$$M = \begin{bmatrix} -1 & -z_0 & c - y_0 \\ z_0 & -\beta & x_0 \\ \sigma & 0 & \sigma \end{bmatrix}. \tag{7}$$

The characteristic equation evaluates at any equilibrium point $E(x_0, y_0, z_0)$ is obtained by solving the equation $\mathrm{Det}(M - \lambda I_3) = 0$, where are the eigenvalues of the system at the equilibrium point and I_3 *is* the 3×3 identity matrix. After solving the above equation, we obtain the characteristic polynomial as follows:

$$\begin{aligned} &-\lambda^3 + (-\beta + \sigma - 1)\lambda^2 + \left(\beta\sigma - \beta + \sigma - z_0^2 + c\sigma - y_0\sigma\right)\lambda \\ &+ \left(z_0^2\sigma - y_0 x_0 \sigma + \beta\sigma + \beta\sigma c - y_0\beta\sigma\right) = 0. \end{aligned} \tag{8}$$

Based on the Routh–Hurwitz criterion, the real parts of all the roots of equation (8) are negative if and only if $(-\beta + \sigma - 1) > 0$ $(\beta\sigma - \beta + \sigma - z_0 + c\sigma - y_0\sigma) > 0$, $(z_0^2\sigma - y_0 x_0 \sigma + \beta\sigma + \beta\sigma c - y_0\beta\sigma) > 0$. This latter equation provides the range of parameter for the equilibrium point to be unstable and generate interesting dynamics.

The trivial equilibrium point is chosen as $E_0(0\ 0\ 0)$, the eigenvalues associate in this case are given as $\lambda_1 = -\beta$, $\lambda_2 = ((\sigma - 1) - \sqrt{(\sigma - 1)^2 + 4\sigma(1 + c)})/2$, and $\lambda_3 = ((\sigma - 1) + \sqrt{(\sigma - 1)^2 + 4\sigma(1 + c)})/2$, but we know that $\beta > 0$, $\rho > 0$ and $\sigma > 1$. The system has three eigenvalues, and the three values do not have the same sign: one of them (λ_3) is positive and the rest is negative mining that when we perturbate the system around that equilibrium point, we can easily use the model to exhibit chaotic phenomena. Those three eigenvalues at E_0 are given as $\lambda_1 = -0.35$, $\lambda_2 = -8.2761$, and $\lambda_3 = 9.9261$; the rest of system parameters are $\sigma = 2.65$, $\beta = 0.35$, and $c = 30$.

4. Numerical Simulation

The evolution of the root of equation (6c) is showing in Figure 1.

In the light of Figure 1, equation 6c can present one, two, or three roots which correspond to the equilibrium points of system (4a–4c) with regard to the parameter T_3.

We observed that, when the load torque changes, the values and the number of equilibrium points resulting in different dynamic of the system also vary. The last equilibrium point is negative by increasing the charge (Figure 1(a)) and positive in Figure 1(b).

In fact, for $T_3 < T_{3max} \approx 2.53698$, there are three nonsymmetric equilibrium points. For $T_3 = T_{3max}$, there are two equilibrium points, while only a single equilibrium point exists for $T_3 > T_{3max}$. Throughout this work, attention is paid to the interesting situation where the system develops three equilibria (i.e., when $0 < T_3 < 2.53698$). It should be noted that, for $T_3 = 0$, the system has three symmetric equilibrium points including the origin.

In the next section, the numerical study of system (4a–4c) is considered. For this purpose, equation (4a–4c) is solved by mean of 4^{th} order Runge–Kutta algorithm [33] with discrete time of 0.005s and the parameter in the range

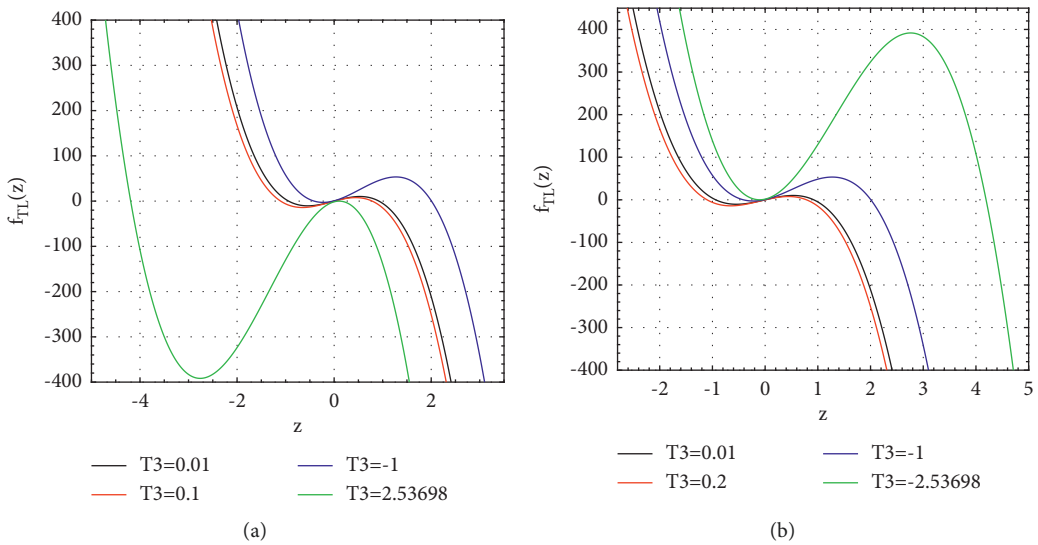

FIGURE 1: Dynamical behaviors of equations (6a–6c) when the parameters are $\sigma = 1.57$; $\beta = 0.03$; $u = 0.009$; $c = 30$; and $\nu = 0.005$.

obtained in the previous section. The bifurcation diagrams of 1-D and 2-D, the maximum Lyapunov exponent plots, the time traces and phase portraits are considered. It should be note that for the maximum Lyapunov exponent plot, positive value represents a chaotic behavior, while negative and zero values represent regular motion of the studied system.

4.1. 2-D Bifurcation Diagram. In this section, the sensitivity of the PMSM versus 2 twin parameters (β, c) or (σ, c) is varied simultaneously in the objective to obtain an overall behavior of the dynamic of the system. We plot the 2-D bifurcation diagrams as shown in Figure 2 with initial states (0.01, 0.01, 20).

The right column of the graphs shows the color indication of the qualitative behavior of the system in accordance with the MLE. Negative and zero values are colored in blue and green; positive values in the other hand are colored in cyan, yellow to red. This graph is very important to engineers specially to indicate the parameter of the PMSM to get a particular dynamic.

For this paper, we choose $c = 30$. It is the zone where various and major phenomena occur, and we draw the 1-D bifurcation diagram to sense the system towards one parameter.

4.2. 1-D Bifurcation Diagram: Sensitivity of the System versus Single Parameter. In this section, the sensitivity of system (4a–4c) versus the parameter σ and the load torque T_L is tested. We fixed the bifurcation parameter using Figure 2, the system is solved for a long time, and the transient is discarded. We record the local maxima of the state variable x and increase in tiny steps the bifurcation parameter. These steps are operated until the last values of the parameter σ. For each value of the bifurcation parameter, we computed the MLE using the well-known Kantz algorithm [34] and draw the graphs.

4.2.1. Sensitivity towards σ. In the light of Figure 3, one can see that the PMSM is chaotic from the set of σ ranging from 1 to 1.5 and 2.9 to 3.2. In the rest of the interval of σ, the system is periodic.

Some phased portraits are drawn for the reader in Figure 4 to let him discovered the final state attractor corresponding to the dynamics observed above.

The reader can notice the well-known period doubling route to chaos in Figure 4a period-a; (b) period-2; (c) period-4; and (e) or (*f*) chaos. The following time traces deeply illustrate the chaos and periodic motion of the PMSM when σ is varied.

4.2.2. Sensitivity towards Constant Lord Torque. In this section, we use the approach where the load torque is constant in all the process driving by the PMSM. The amplitude of the load torque highlights some unobserved streaking dynamical behaviors. We choose $\sigma = 1.5$ and $c = 30$, with the help of 2-D bifurcation diagram of Figure 2. The bifurcation diagram obtained by plotting the local of the state variable x versus the amplitude of the constant load torque T_3 is shown in Figure 5.

The chaotic behavior shown in Figure 5 illustrates that the phase portrait of system (4a–4c) for specific value of T_L is always chaotic with some periodic windows sandwiches inside chaotic intervals. This phenomenon is named intermittency route to chaos. This striking dynamic was first discovered by [35]. Recently, they are found in thermoacoustic oscillations [36] in biochemical systems [37], in electronics jerk oscillators [38], and just to name a few. This dynamic that appears in this type of system constitute a major contribution, therefore, need to be shared. As we can see in Figure 6, the phase portraits drawn for some discrete values of the load torque showing how the attractor is chaotic and then become periodic suddenly.

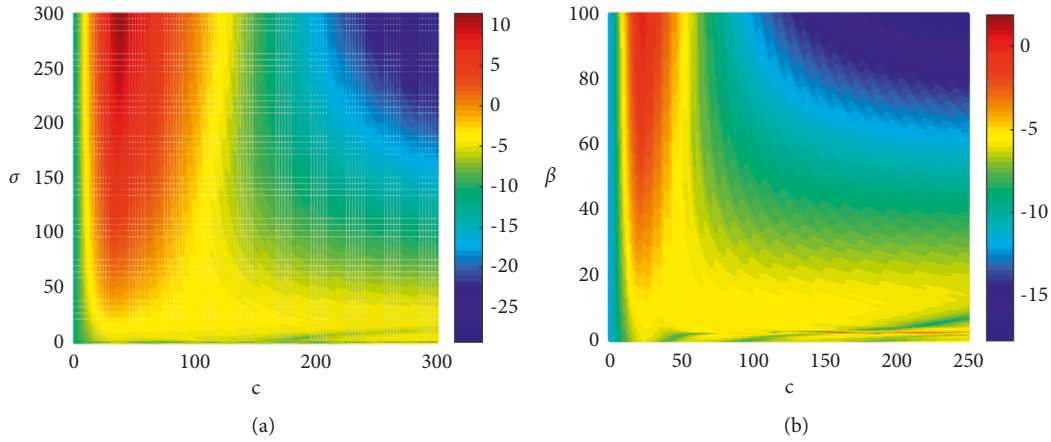

FIGURE 2: 2-D bifurcation diagrams showing the dynamics of system (4a–4c) by varying two different parameters simultaneously. The right column bar represents the value of the MLE. (a) σ and c; (b) β; and (c) the rest of the parameters of the systems are (a) $u = 0.009$; $\beta = 0.03$; $v = 0.005$; and $T3 = 0.01$; (b) $u = 0.009$; sigma = 2.65; $v = 0.005$; and $T_3 = 0.01$; the initial conditions are $x = 0.01$; $y = 0.01$; and $z = 20$.

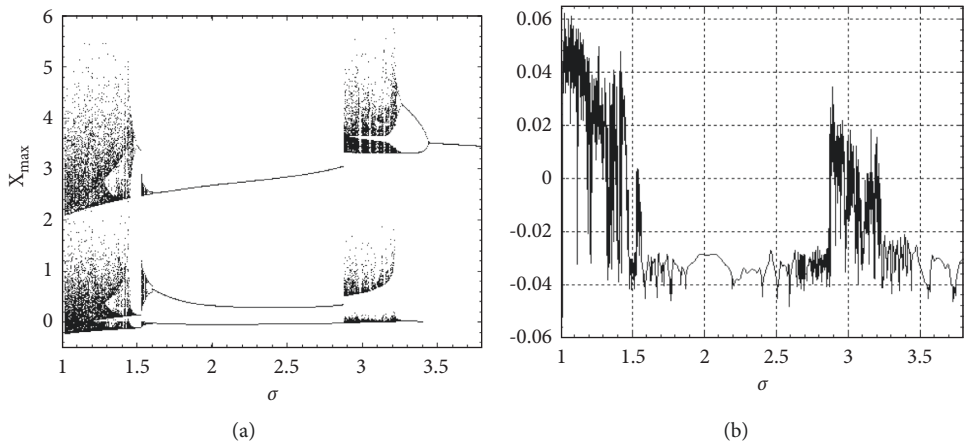

FIGURE 3: Bifurcation diagram and the corresponding maximum Lyapunov exponent $L = L_d = L_q = 1.99$ MHz, $R = 0.9\,\Omega$ $k_t = 0.049$Nm/A, $J = 5{\times}10^{-6}$kgm^2, $b = 2.3{*}10^{-2}$ N/rad/s, and $c = 30$; σ (1 to 3.8); $u = 0.009$; $\beta = 0.03$; $v = 0.005$; $T_3 = 0.01$; the initial conditions are $x = 0.01$; $y = 0.01$; $z = 20$.

4.2.3. Sensitivity towards Amplitude of a Continuous Varying Lord Torque. In this section, we use the approach case where the load torque is sinusoidal in all the process driving by the PMSM. The amplitude of the load torque highlights some unobserved streaking dynamical new phenomena. In the industry, some load applied to the PMSM is nonconstant but varies continuously [39, 40]. To mimic this type of load, we introduce here a sinusoidal load as follows.

$u = T_3 * \sin(2 * \pi * F * t)$ where T_3 is the amplitude of sinusoidal torque; F is its frequency and t is the time. We then change it to a squared wave form in the next section. The local waveform of the torque is given in Figure 7.

The bifurcation and the local maximum exponent plot of the PMSM, when the load torque of sinusoidal waveform, is given in Figure 8.

Figure 8 shows that under certain values of the amplitude of the load torque, the system is chaotic and periodic for some others. The main remarks here are that the diagrams differ from the ones in Figure 3. To deep inside this result, the times series and phase portraits plotting in this case in (x; y) plan are shown as follows for $\sigma = 1.56$.

The system exhibits periodic and chaotic dynamics under a set of system parameter selected in the caption of Figure 9. By changing the value of the amplitude of sinusoidal load torque, the phase portrait confirms the behaviors shown by the bifurcation diagram. We also notice that the attractors are always double-scroll in contrast to the one in Figure 10, where they are some of one scroll.

Because the square load torque is a king of nonsinusoidal wave, we consider that the square torque is the sum of many waves with many frequencies, we use that form of signal torque to evaluate the behaviors of the machine under this condition.

Bursting phenomena are observed in the system when the load torque is sinusoidal. The curve describing those behaviors obtained by changing the amplitude of the signal is given in Figure 11.

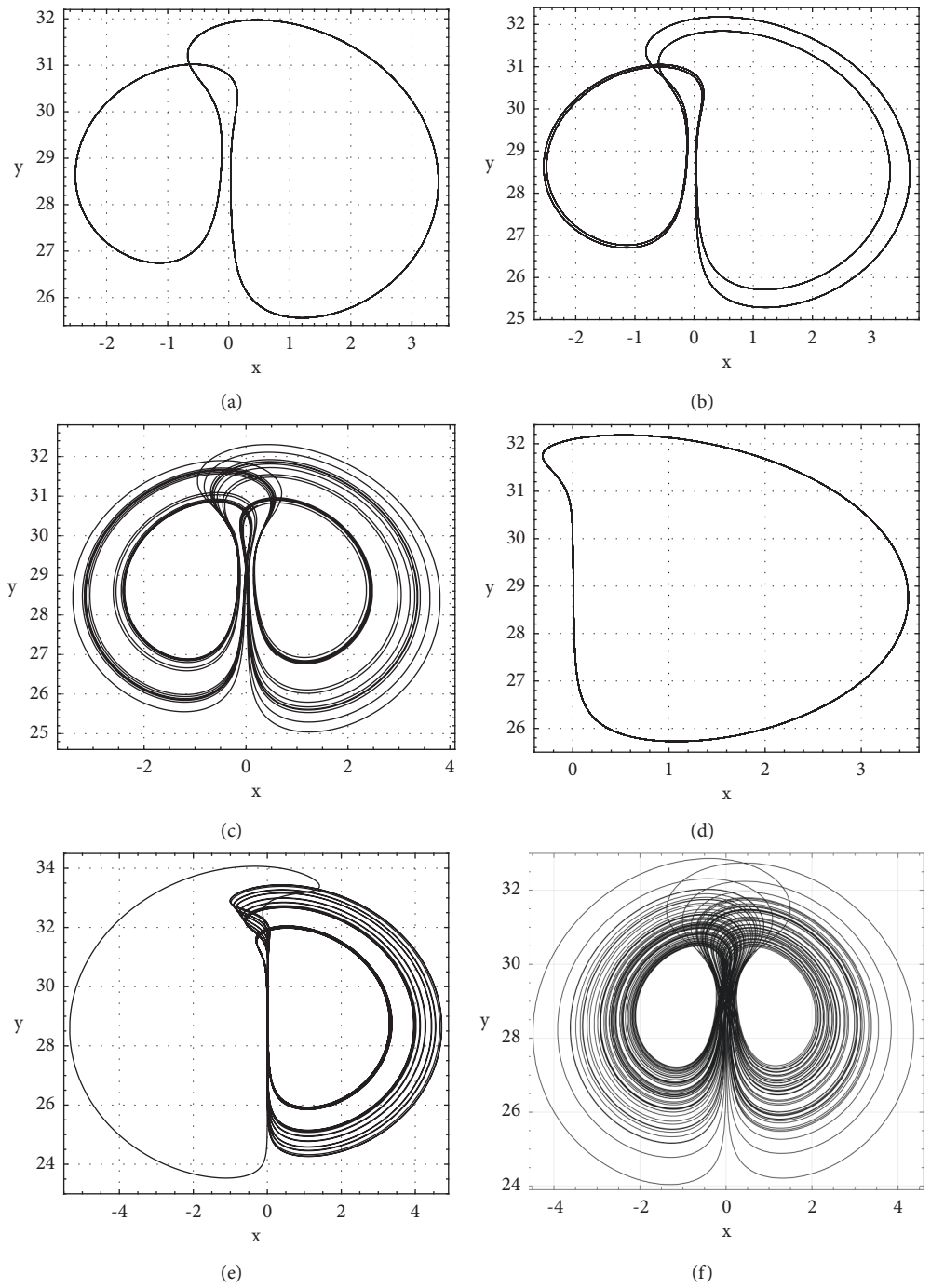

Figure 4: The phase portraits of system (a–c) in planes (x, y) for specific value of σ: (a) $\sigma = 1.5$, (b) $\sigma = 1.479$, (c) $\sigma = 1.32$, (d) $\sigma = 3.5$, (e) $\sigma = 3.199$, and (f) $\sigma = 1.025$; the initial conditions are (0.01, 0.01, 20). The system parameters are $c = 30$; $u = 0.009$; $\beta = 0.03$; $\nu = 0.005$; $T_3 = 0.01$.

As announced in this section, we use the approach case where the load torque is square in all the process driving by the PMSM. In the presented of the square load torque in particular the amplitude of the load torque highlights some unobserved streaking dynamical new phenomena; therefore, they need to be shared. The form of the time series square load torque is given as $u = T_3 * \text{square}\ (2 * \pi * F * t)$; the local form is given in Figure 12.

We show that under the condition above, the system exhibits period one, double-scroll, and chaotic attractor. The phase portraits are given in Figure 14.

The figures confirm the behaviors described by the bifurcation diagram: periodic and chaotic attractors.

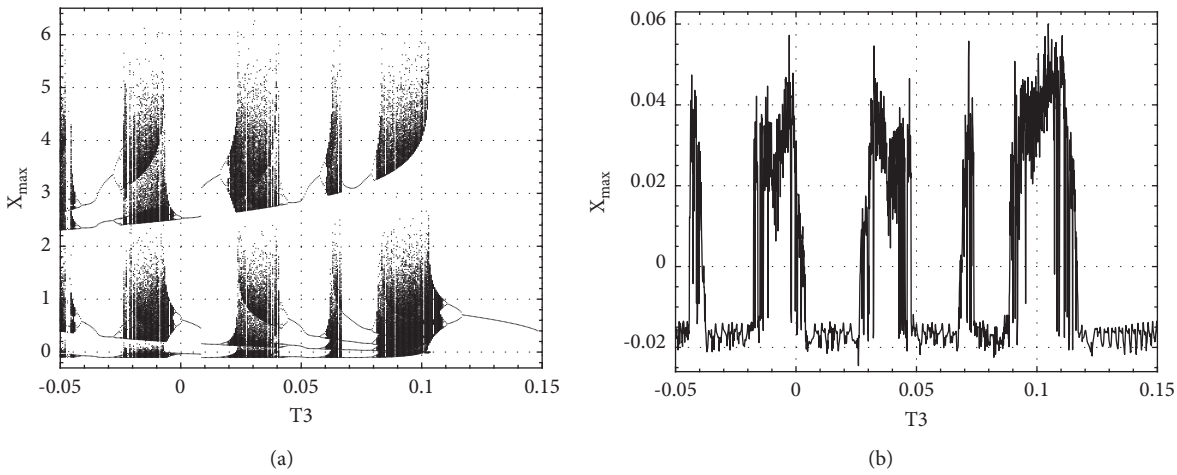

Figure 5: Bifurcation diagram (a) and its corresponding graph of MLE (b) of the motor by variation of the constant load torque. $C = 30$; $u = 0.009$; $v = 0.005$; beta $= 0.03$; $\sigma = 1.65$. The initial conditions are $x = 0.01$; $y = 0.01$; $z = 20$.

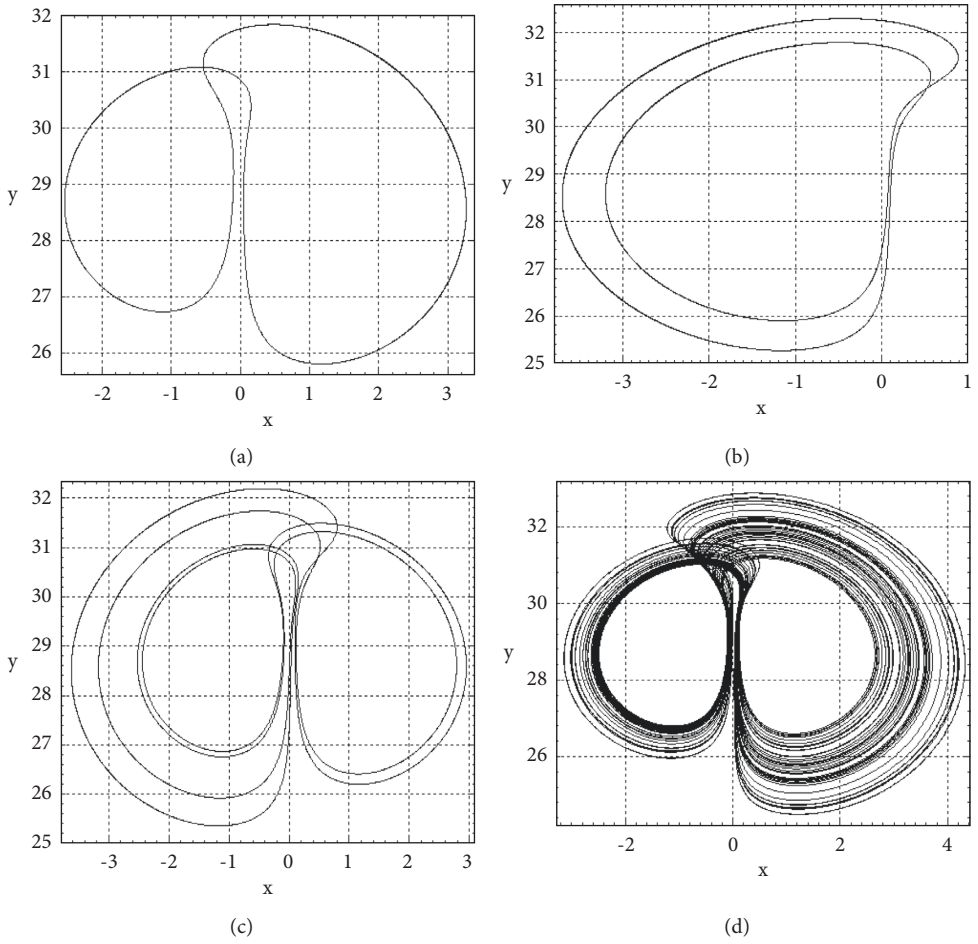

Figure 6: Continued.

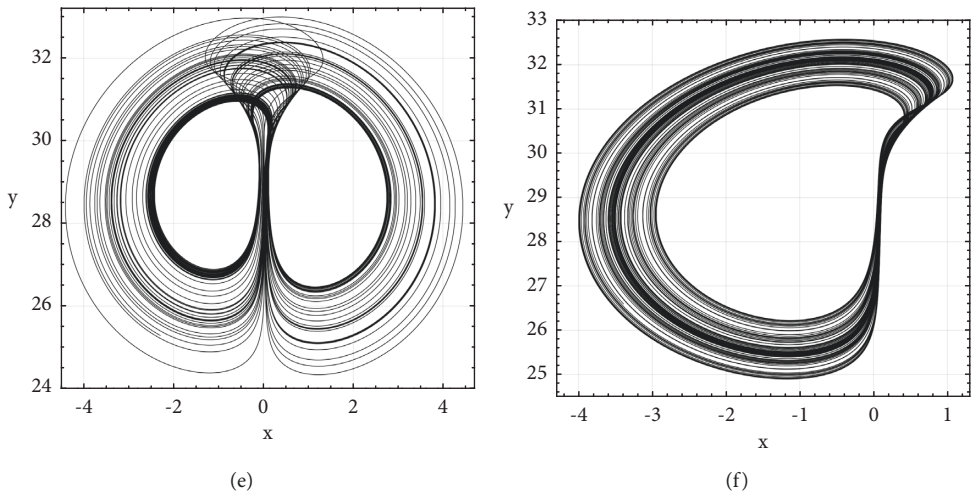

Figure 6: Phase portraits of system (4a–4c) in planes (x, y) for specific value of T_3: (a) $T_3 = 0.02$, (b) $T_3 = 0.12$, (c) $T_3 = 0.05$, (d) $T_3 = 0.03$, (e) $T_3 = 0.045$, and (f) $T_3 = 0.1148$. Initial conditions are (0.01, 0.01, 20) the system parameters are $c = 30$; $u = 0.009$; $\beta = 0.03$; $\nu = 0.005$; $\sigma = 1.65$. We can see that the phase portraits (b) and (f) display intermittency behavior.

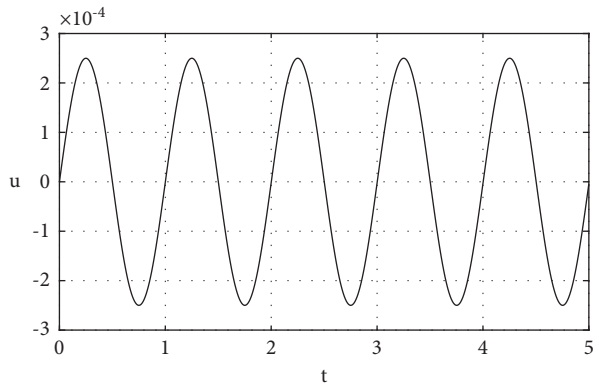

Figure 7: Sinusoidal waveform of the load torque $T_3 = 0.00025$; $F = 1$ Hz.

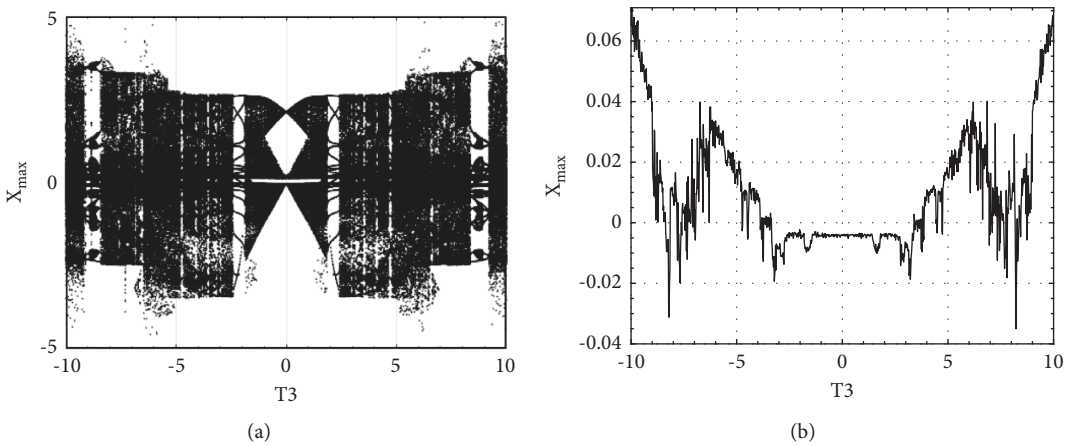

Figure 8: Bifurcation diagram (a) and the corresponding largest Lyapunov Exponent (b) of the PMSM driving a sinusoidal load torque by variation of the amplitude (A) $F = 1$ Hz; initial conditions are ($x_0 = 0.01$; $y_0 = 0.01$; $z_0 = 20$); and the other parameters of the system are $c = 30$; $u = 0.009$; $\nu = 0.005$; $\beta = 0.03$; $\sigma = 1.56$.

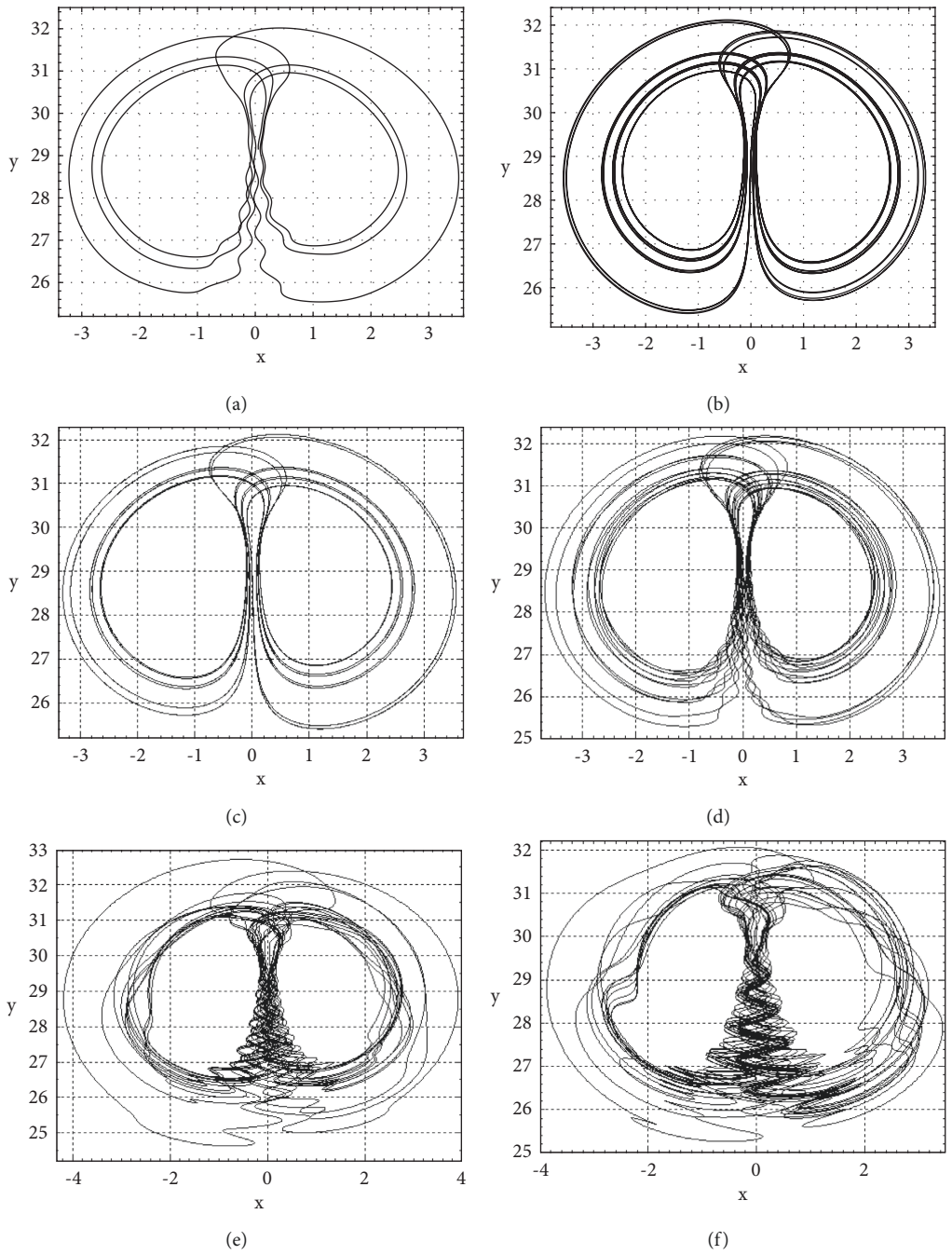

Figure 9: Phase portraits plotted for $F = 1$ Hz; the initial conditions are ($x_0 = 0.01$; $y_0 = 0.01$; $z_0 = 20$); the system parameters are $c = 30$; $u = 0.009$; $v = 0.005$; $\beta = 0.03$; $\sigma = 1.56$; (a) $A =$ -1.0259, (b) $A = -4.6959$, (c) $A = 0.02$, (d) $A = 1$, (e) $A = -5$, and (f) $A = -8.5$.

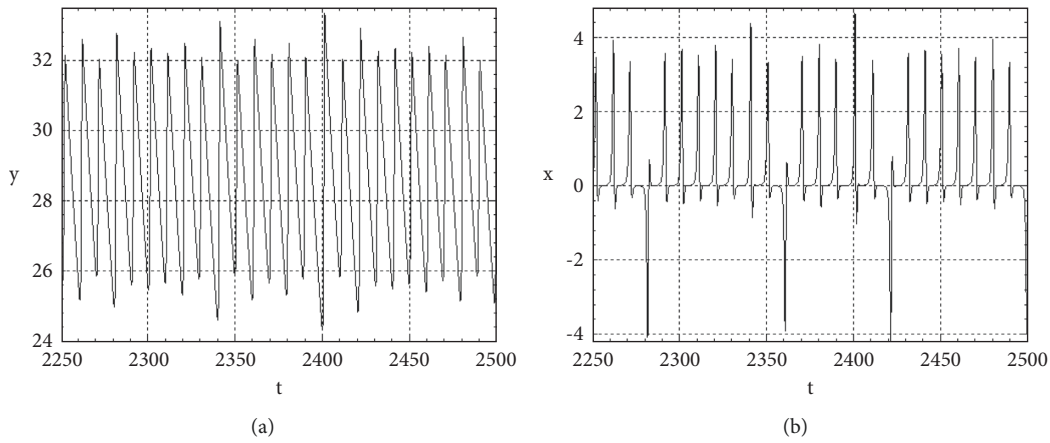

Figure 10: The time series of system (4a–4c) for specific value of σ parameter. The other parameters are $c = 30$; $u = 0.009$; $\beta = 0.03$; $\nu = 0.005$; $T_3 = 0.01$; initial conditions are (0.01, 0.01, 20).

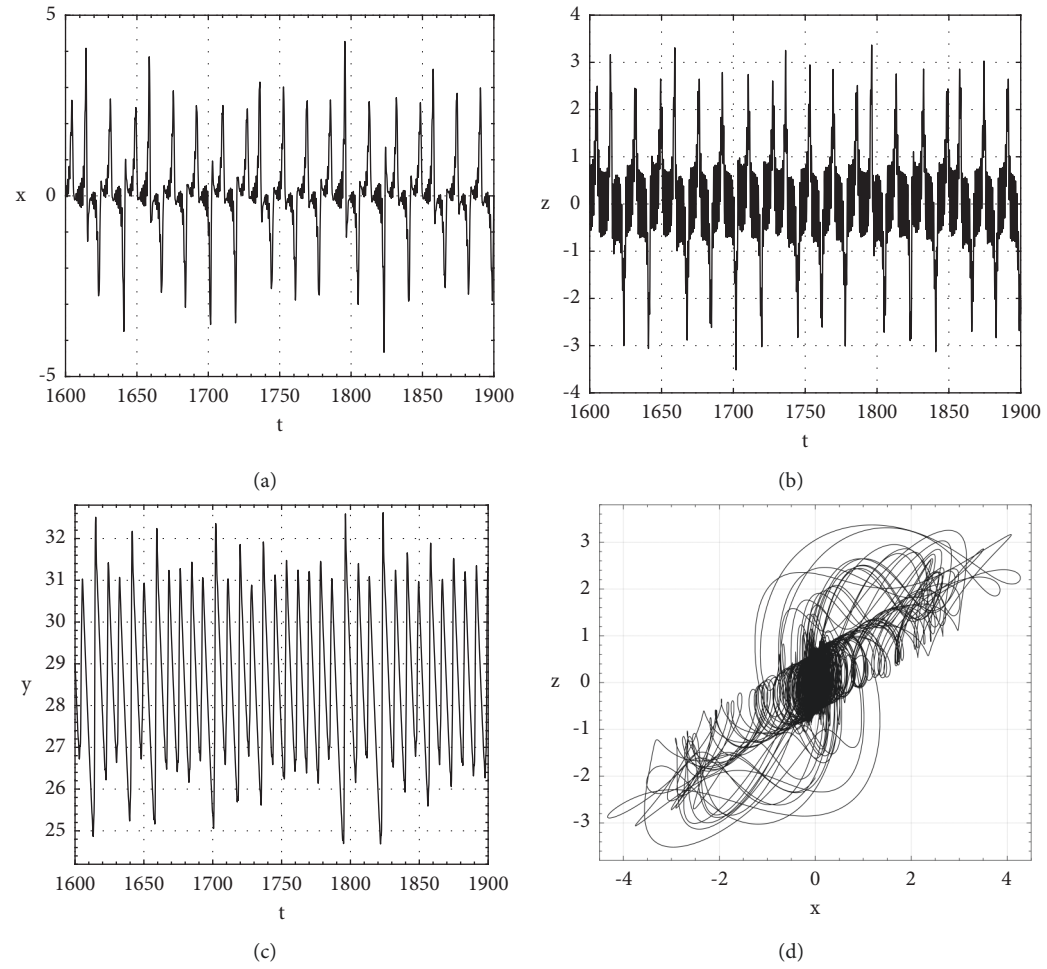

Figure 11: Time series (a), (b), (c), and phase portrait in plant (z, x) (d) of bursting phenomena obtained when the amplitude of the sinusoidal load torque is $T_3 = 4.6959$. The frequency is $F = 50$ Hz, and the rest of parameters are the same as in Figure 9.

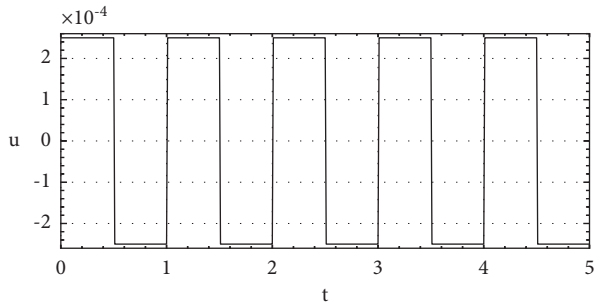

Figure 12: Time series of the square load torque when $T_3 = 0.00025$, $F = 1$ Hz, when the load torque has a square form, we obtained the bifurcation diagram and the local maximum exponent by varying the amplitude of the signal as given in Figure 13.

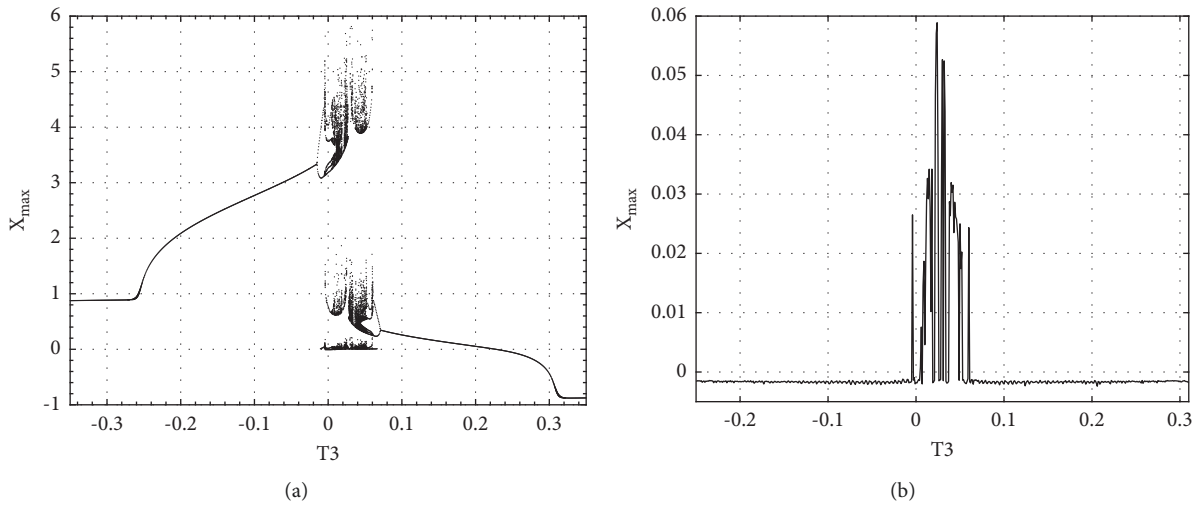

Figure 13: Bifurcation diagram and the local maximum exponent of the motor when the load torque is a square waveform. *F = 1 Hz*; initial conditions (*x0 = 0.01; y0 = 0.01; z0 = 20)*; $c = 30$; $u = 0.009$; $v = 0.005$; beta = 0.03; $\sigma = 3.05$.

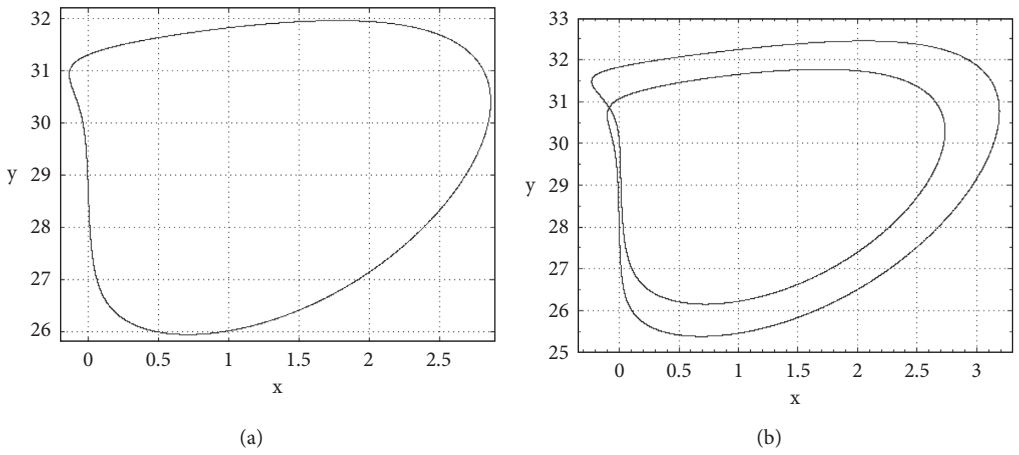

Figure 14: Continued.

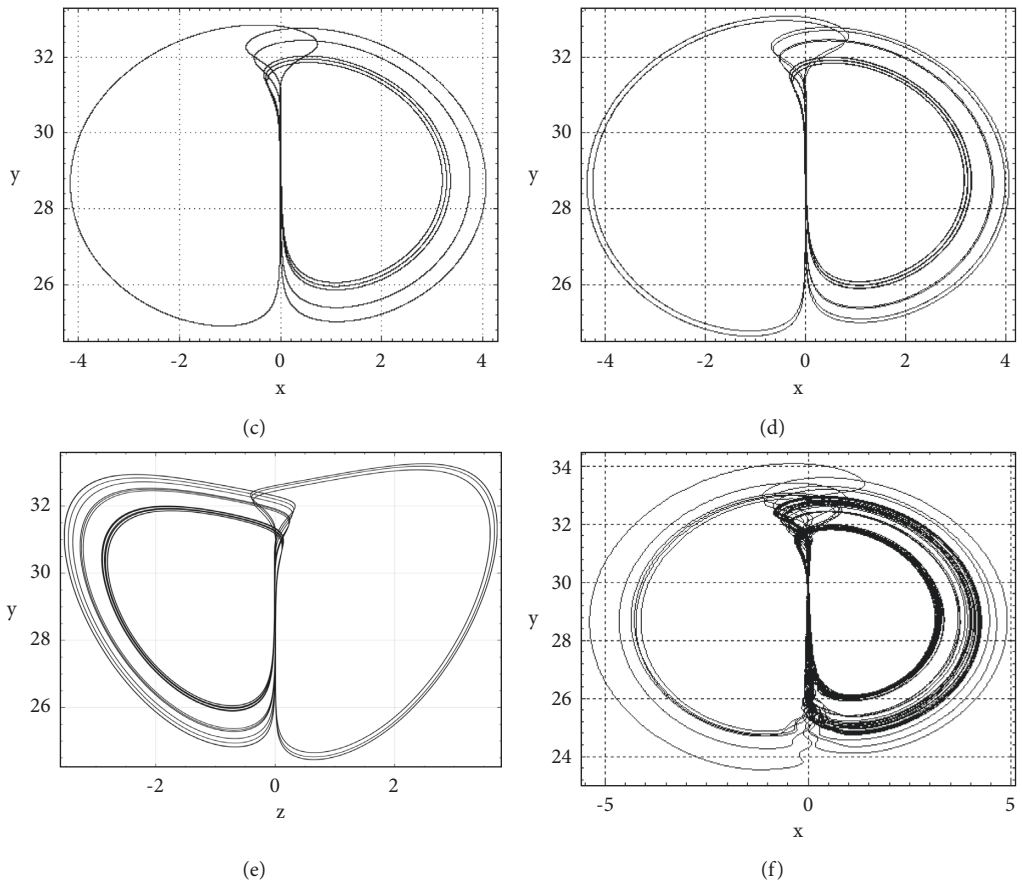

Figure 14: Phase portraits plotted showing the sensitivity of the system towards squared amplitude of the load torque: $F = 1$ Hz; $x0 = 0.01$; $y0 = 0.01$; $z0 = 20$; h:0.005; $c = 30$; $u = 0.009$; $v = 0.005$; beta = 0.03; $\sigma = 3.105$; (a) $T_3 = -0.02$, (b) $T_3 = -0.012$, (c) $T_3 = 0.001$, (d) $T_3 = 0.05$, (e) $T_3 = 0.05$, and (f) $T_3 = 0.055$.

5. Circuit Implementation of the PMSM

The physical feasibility and existence of chaos attractors in system (1a and 1b) are tested in this section by designing an analog electronic circuit. Many tools have been used accordingly by researchers including MULTISIM, OrCAD-PSpice, or PSIM just to name a few [41–44].

Note that OrCAD-PSpice is an advanced analysis technology combining industry-leading, native analog, mixed-signal, and analysis engines to deliver a complete circuit simulation and verification solution. Its technology provides the best, high-performance circuit simulation to analyze and refine your circuits, components, and parameters before committing to layout and fabrication. Therefore, the hardware implementation of the circuit is relevant in technological applications including chaos-based communications, random signal generation, image encryption, and so on. The schematic diagram of Figure 15 has been simulated in OrCAD-PSpice software, and it represents the analog circuitry of system (4a–4c). This structure is exclusively based on diodes, resistors, capacitors analog multiplier, and few operational amplifiers. This is the more appropriated way to realize analog operations.

To applying Kirchhoff's electric laws on the circuit, the following set of three coupled first-order nonlinear differential equations are obtained:

$$C_1\frac{dV_x}{d\tau} = \frac{-Vx}{R_{35}} + \frac{Vz}{R_{34}} + \frac{-VyVz}{R_{24}} + \frac{V_9}{R_{39}}, \tag{9a}$$

$$C_2\frac{dV_y}{d\tau} = \frac{-Vy}{R_{36}} + \frac{VxVz}{R_{27}} + \frac{V_{10}}{R_{38}}, \tag{9b}$$

$$C_3\frac{dV_z}{d\tau} = \frac{-Vz}{R_{37}} + \frac{Vx}{R_{21}} + \frac{V_8}{R_{40}}, \tag{9c}$$

where V_x, V_y, and V_z are the output voltages of the operational amplifiers. In order to recover original system (4a–4c), the voltages and time can be normalized as follows:

$$\begin{aligned} V_x &= x.1V, \\ V_y &= y.1V, \\ V_z &= z.1V, \frac{t}{RC} = \tau. \end{aligned} \tag{10}$$

Then, after substitution of equation (10) into equations (9a–9c), one can obtain the following set of differential

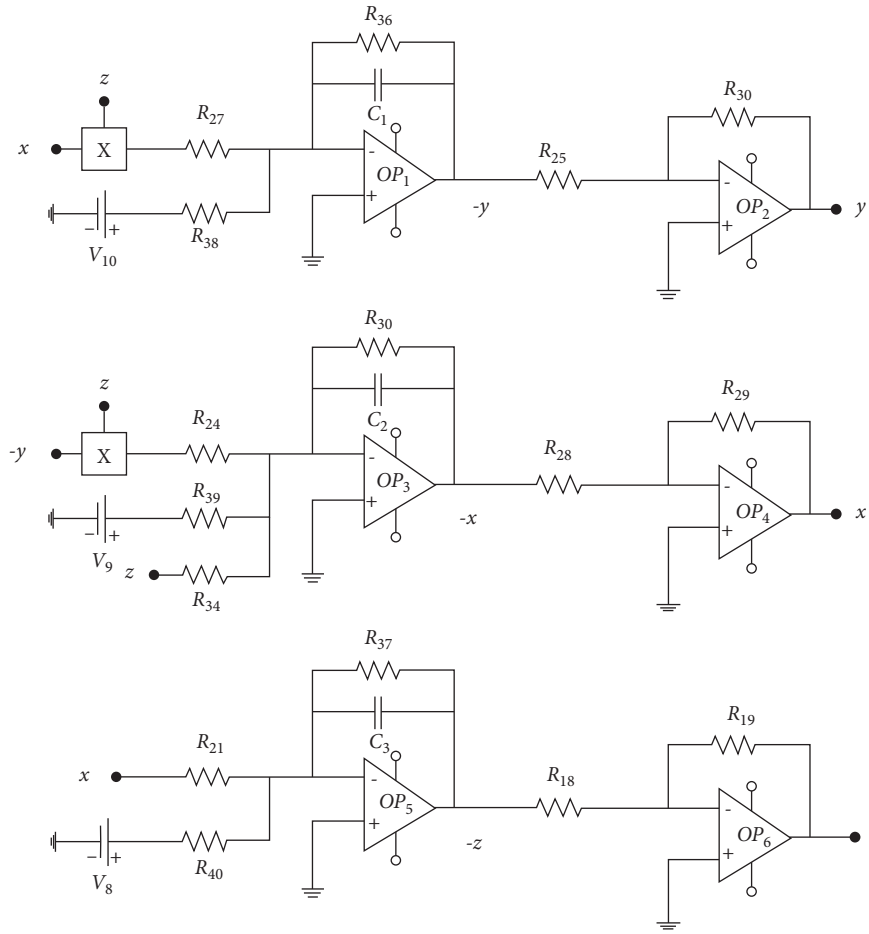

Figure 15: The schematic diagram of the PMSM described by system (1a and 1b).

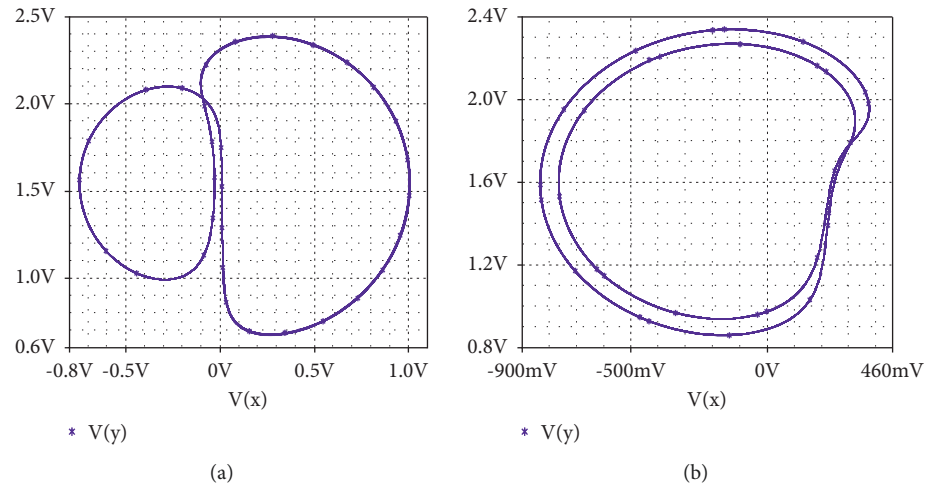

Figure 16: Continued.

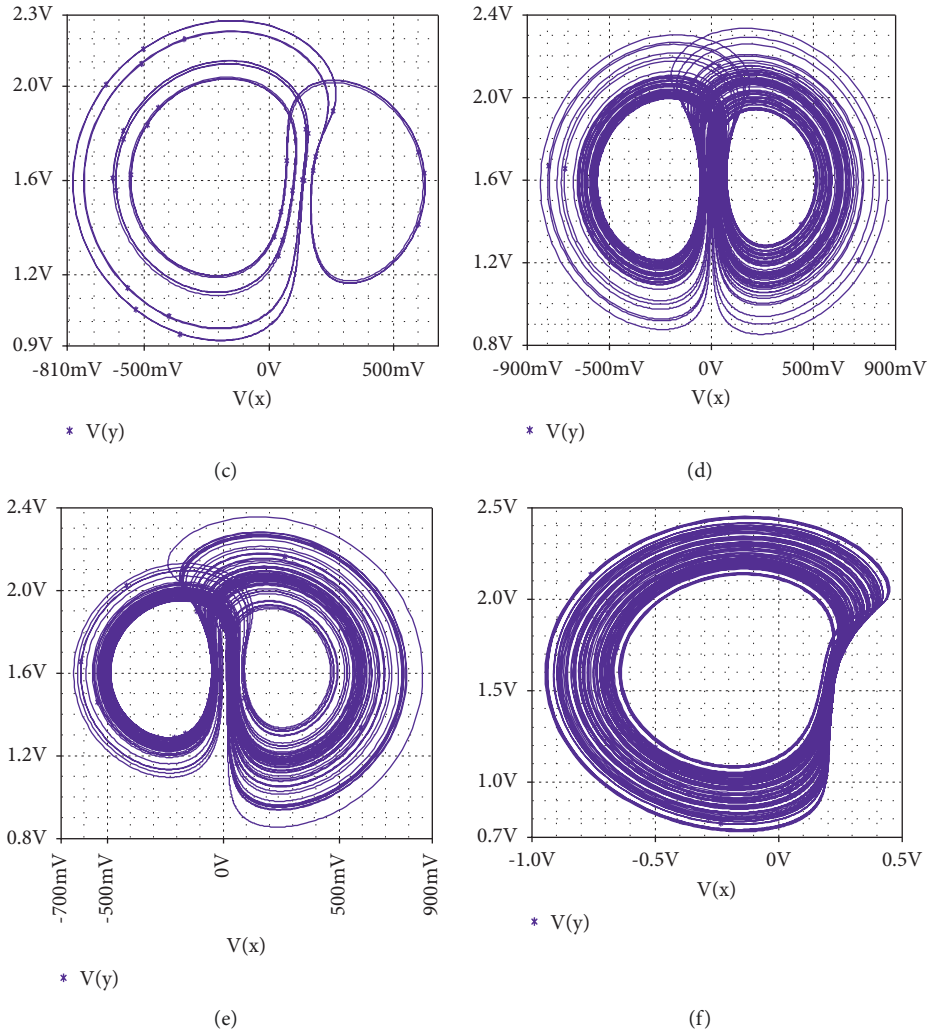

FIGURE 16: The phase portraits of the chaotic attractor and periodic attractor in planes (V_x, V_y) observed on the OrCAD-PSpice. The initial conditions are $V_x(0) = V_y(0) = V_z(0) = 0.01V$. The values of the resistors and capacitors are $R_{27} = R_{21} = 10k\Omega$, $R_{38} = 150M\Omega$, $R_{39} = 60M\Omega$, $R_{34} = 6k\Omega$, $R_{21} = R_{37} = 10.8521k\Omega$, $R_{36} = 150k\Omega$, $R_{35} = 100k\Omega$, $R_{28} = R_{29} = R_{18} = R_{19} = R_{25} = R_{30} = 1k\Omega$, $C_1 = C_2 = C_3 = 10nF$, $V_7 = V_8 = V_9 = V_{10} = 15V$ $R_{40} = R_A$: (a) period-1 attractor $R_A = 14.021\,\text{M}\Omega$, (b) periodic $R_A = 450\text{k}\Omega$, (c) periodic $R_A = 750\text{k}\Omega$, (d) chaotic attractor $R_A = 41955.22\,\text{k}\Omega$, (e) chaotic attractor $R_A = 4781\text{k}\Omega$, and (f) chaotic attractor $R_A = 480\,\text{k}\Omega$.

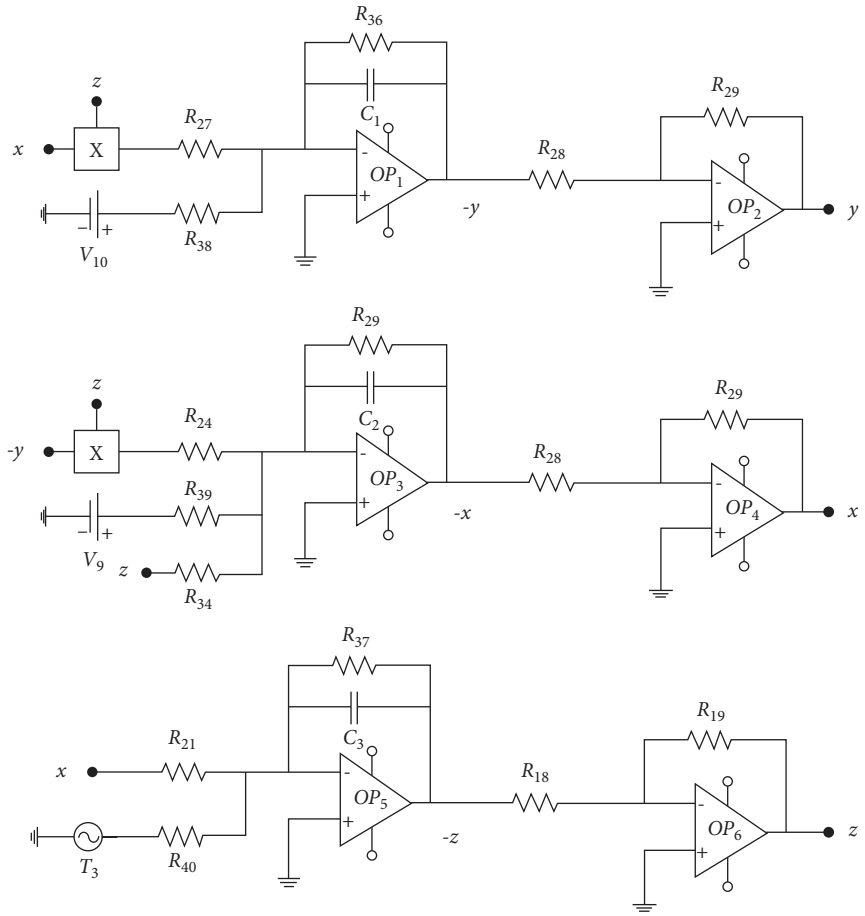

Figure 17: Circuit diagram with the sinusoidal torque driven by the PMSM.

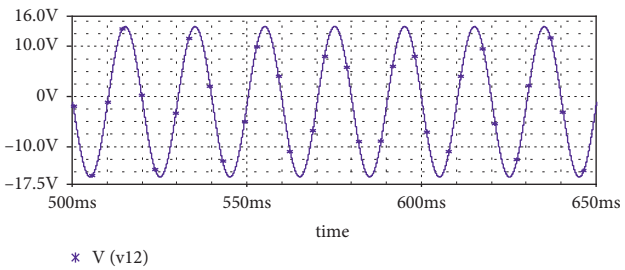

Figure 18: Sinusoidal waveform of the load torque driven by the PMSM. $A = 15\,\text{V}$, $F = 50\,\text{Hz}$.

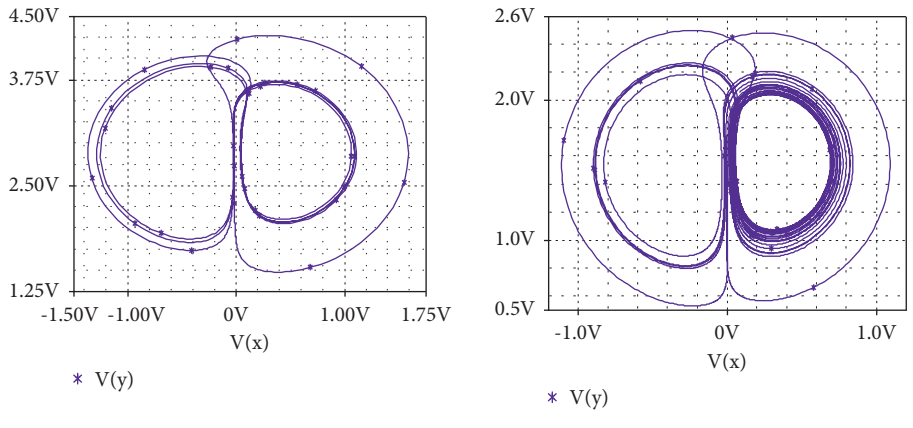

Figure 19: Continued.

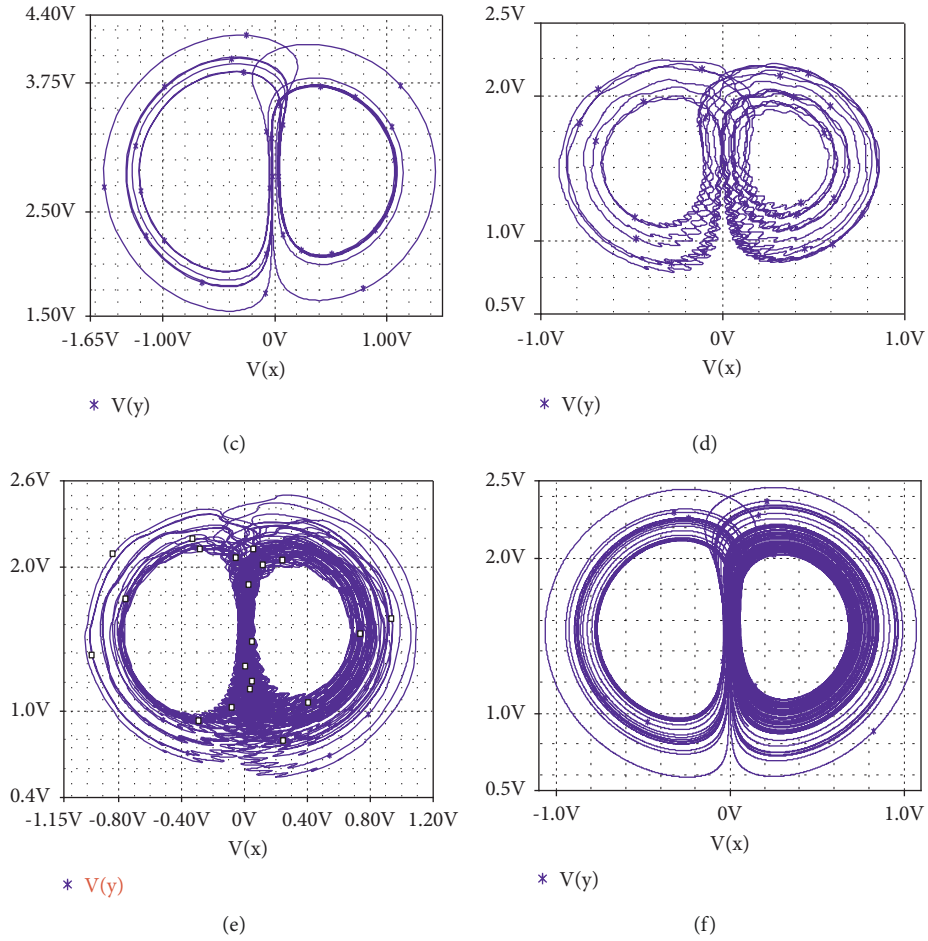

FIGURE 19: Behavior of the electronic circuit describing the motor driving a sinusoidal waveform. The circuit implement in OrCAD-PSpice results in the phased portraits in Figure 19 are captured. We obtained all these forms with the following value of parameters: (a) $R_{40} = 8000\text{k}\Omega$, (b) $R_{40} = 15\text{M}\Omega$, (c) $R_{40} = 12000\text{k}\Omega$, (d) $R_{40} = 800\text{k}\Omega$, (e) $R_{40} = 350\text{k}\Omega$, and (f) $R_{40} = 275.25\,\text{k}\Omega$ and (V = 15V; F = 50 Hz; $R_{21} = R37 = 6.4102564\,\text{k}\Omega$), and the rest of parameters are the same as the ones used to plot Figure 16. We can see that the analytical results are checked experimentally and a very good agreement is found between numerical and experiments data.

equations governing the dynamics of the dimensionless variables x, y, and z:

$$\frac{dx}{dt} = -x - yz + cz + u, \tag{11a}$$

$$\frac{dy}{dt} = -\beta y + xz + v, \tag{11b}$$

$$\frac{dz}{dt} = \sigma(x - z) - T_3. \tag{11c}$$

By comparing system (11a–11c) with system (4a–4c), the following expressions between the parameters and the circuit's components (resistors and capacitors) are obtained:

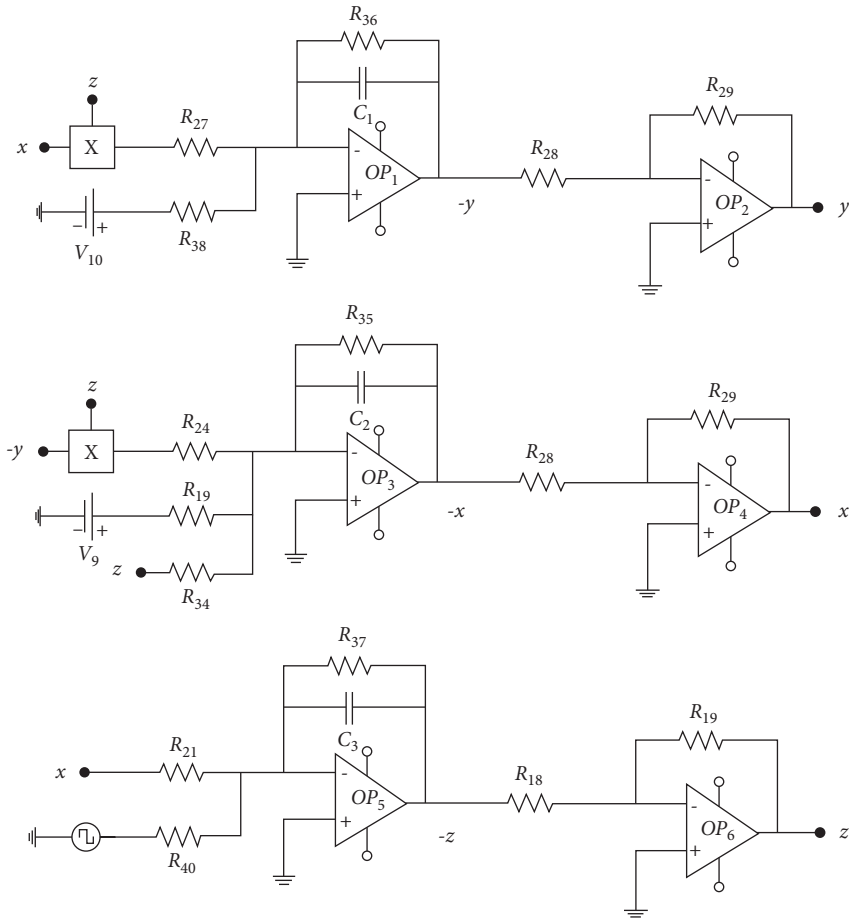

Figure 20: Electronic implement of the square load torque in this machine. The squared load torque is T_3.

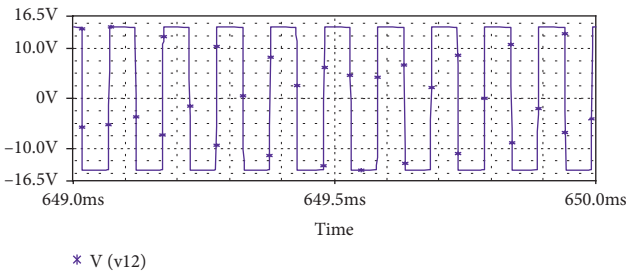

Figure 21: The wave form of square load torque with $R = 5.05\,\text{M}\Omega$.

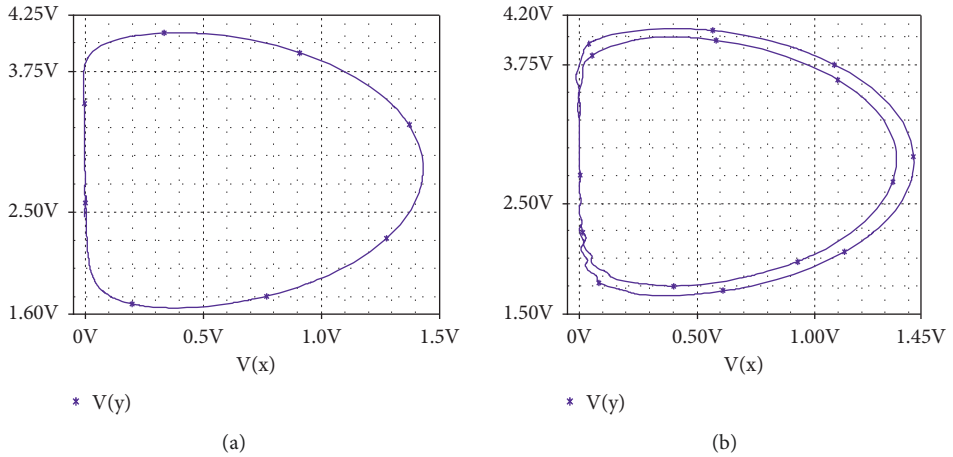

Figure 22: Continued.

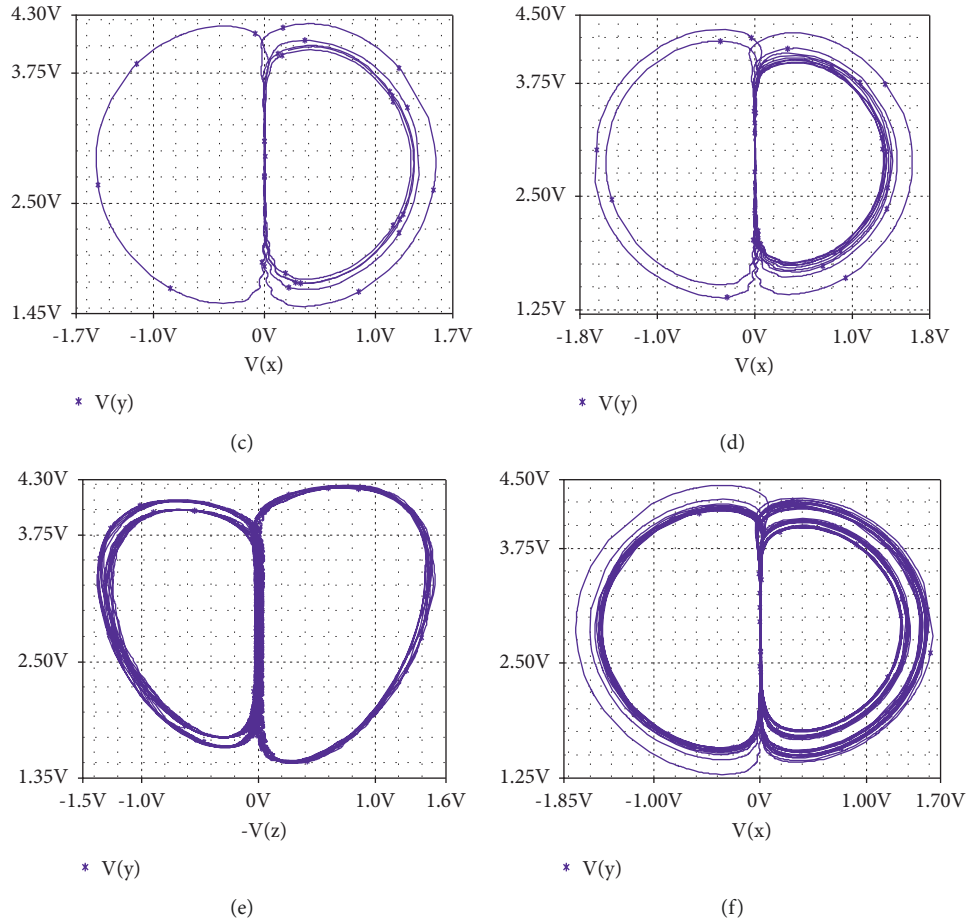

Figure 22: Phase portraits of system (11a–11c) in (Vx, Vy) plane of the circuit in Figure 21 show the behavior of the system obtained in OrCAD-PSpice when the load torque in a square signal. (a) $R_{40} = 500\text{k}\Omega$, (b) $R_{40} = 505.254\,\text{k}\Omega$, (c) $R_{40} = 380.55\text{k}\ \text{k}\Omega$, (d) $R_{40} = 800\text{k}\Omega$, (e) $R_{40} = 850.8\,\text{k}\Omega$, and (f) $R_{40} = 950.698\,\text{k}\Omega$. The initial values of capacitors voltage are $(V_X(0), V_y(0), V_z(0))$= (0.01 V, 0.01 V, 0.01 V), the value of some resistance is $R_{21} = R_{37} = 3.278\,\text{k}\Omega$, and other parameters are unchanged.

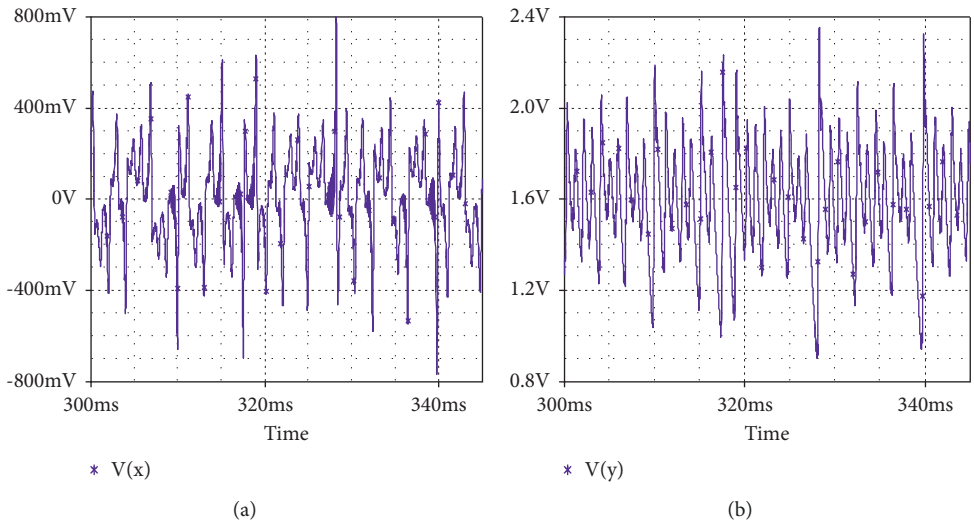

Figure 23: Continued.

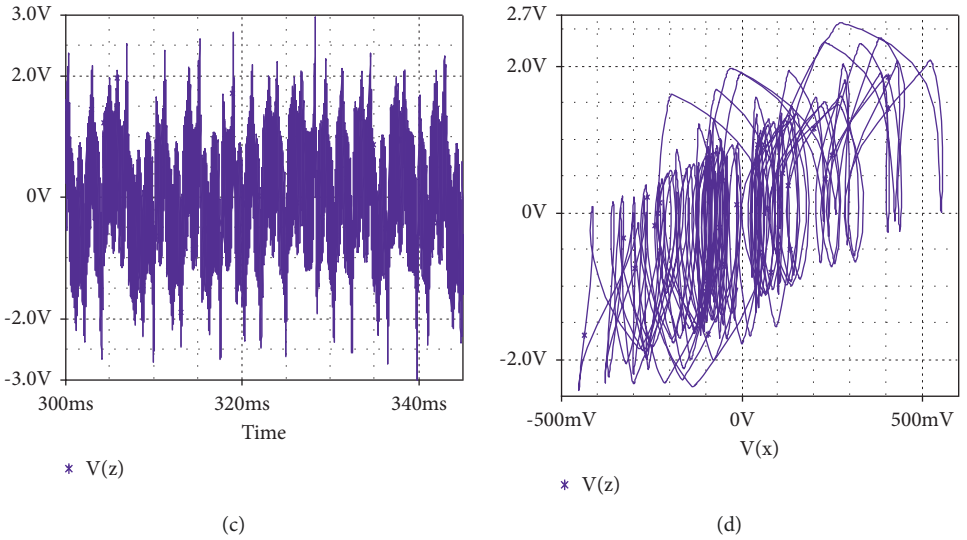

Figure 23: Time series (a), (b), (c), and phase portrait in plant (z, x) (d) of bursting phenomena obtained when the amplitude of the sinusoidal load torque is $R = 35.2154\,k\Omega$, the frequencies is $F = 50\,Hz$, and the rest of parameters are unchanged.

$$\begin{aligned}
\sigma &= \frac{1}{R_{21}},\\
T_3 &= \frac{V_8}{R_{40}},\\
\beta &= \frac{1}{R_{36}},\\
\frac{V_{10}}{R_{38}} &= v,\\
\frac{V_9}{R_{39}} &= u,\\
\frac{1}{R_{34}} &= c,\\
R_{37} &= R_{21}.
\end{aligned} \tag{12}$$

To verify the similarity between numerical results and experimental study, the observations from the OrCAD-PSpice of the phase portraits of the designed circuit of system (11a–11c) are shown in Figure 16.

The phase portraits on Figure 16 resemble the one in Figure 6; this statement shows that the electronic circuit produces the periodic and chaotic attractors found in numerical analyses section (see Figure 6). We can conclude that the circuit describes the dynamic behavior of the machine when the load changes in the constant values. Another analytical results confirmed are the behavior of the system towards sinusoidal load torque. For this purpose, the following OrCAD-PSpice diagram is proposed in Figure 17.

By using the sinusoidal load torque $T_3 = A\sin(\omega t)$, we obtained in OrCAD-PSpice the form of the signal used in Figure 18 as follows.

The attractor form obtained in OrCAD-PSpice is given in Figure 19.

The last result to check is system (11a–11c) driving a squared load torque. In this regards the following diagram in Figure 20 is proposed in OrCAD-PSpice.

Figure 21 shows the time series of the general form of the square function plotting in OrCAD-PSpice.

The phase portraits obtained by variation of the amplitude of the square signal are given in Figure 22.

We see that when the load torque is a square function, the motor exhibits chaotic attractors and conserves the general form of attractors found in numerical findings. Notice that the squared load torque represents an "on-off" (load apply-load not apply) load driven by the machine. This result represents a contribution to the understanding of the dynamic of the PMSM, therefore needs to be shared.

The bursting phenomena are implemented in OrCAD-PSpice when the parameter taking some range of value and the behavior of those phenomena is shown in Figure 23.

Figure 24 illustrates the comparisons of the numerical results phased portraits with the experimental ones.

In the light of Figure 24, it is easy to see that good agreement is met between numerical and experimental studies.

6. Chaos Control of PMSM Motor Using Single Self-Feedback Delay Controller

A single self-feedback delay controller is investigated in this section to stabilize the chaotic behavior found in the PMSM. The details of this method can be found in [15] and other related papers. In order to achieve this goal, the controlleris added to equation (9a) of system (4a–4c):

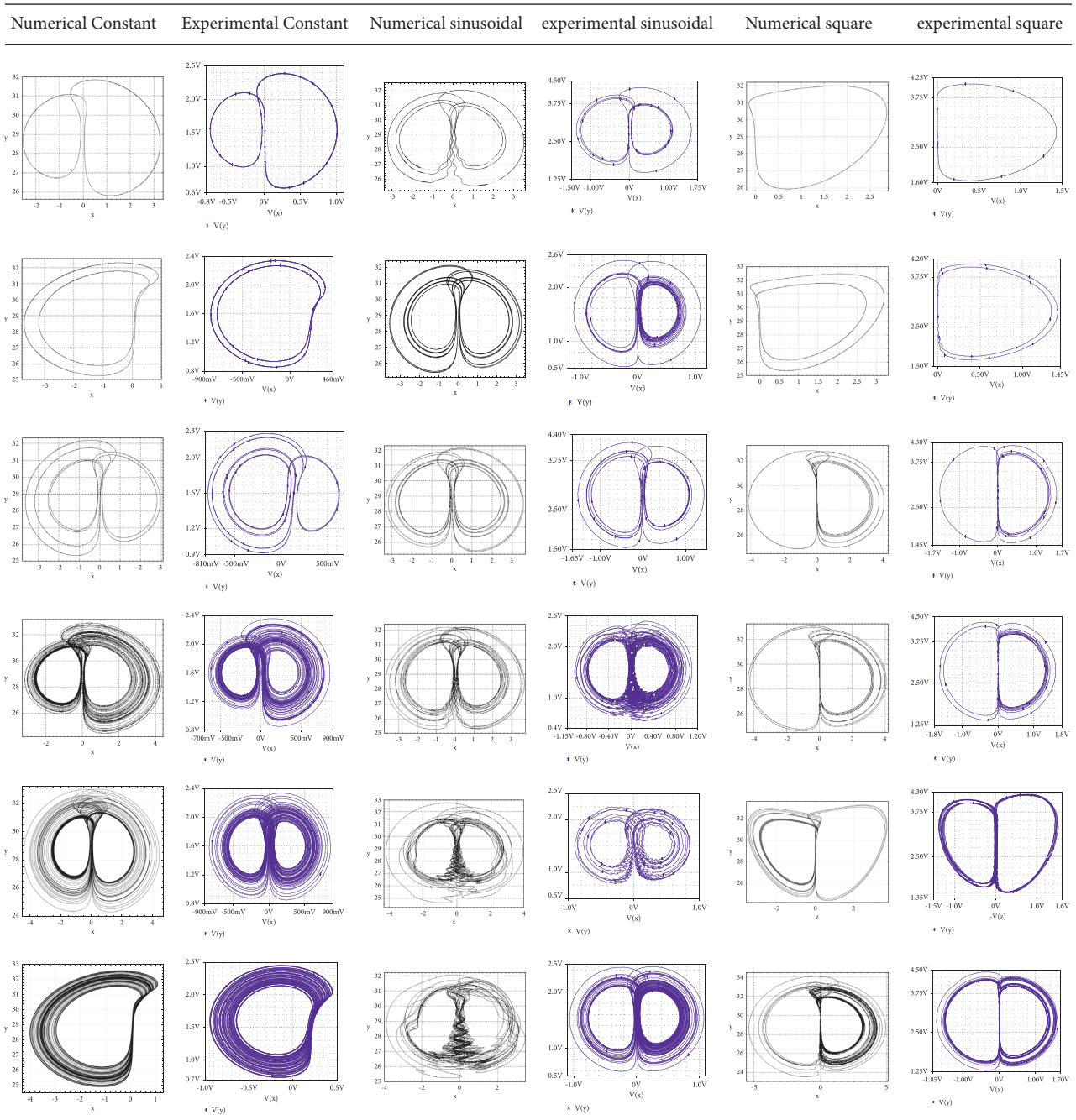

Figure 24: Phased portraits of numerical result compared to experimental studies.

$$\frac{dx}{dt} = -x - yz + cz + u, \tag{13a}$$

$$\frac{dy}{dt} = -\beta y + xz + v + u1, \tag{13b}$$

$$\frac{dz}{dt} = \sigma(x - z) - T_3, \tag{13c}$$

where the controller is $u_1 = kf\,(z(t - to) - z(t))$ with kf is the coupling strength of the controller. The value of the control parameters and the form of curve is given in Figure 25 with $to = 0.5$ and $kf = 0.035$.

It is easy to see that the control system is periodic. Firstly, the behaviors of machine are chaotic with no control ($kf = 0.0$); but when the control function parameters are $to = 0.5$ and $kf \in [0.02 - 0.035]$, the system becomes periodic.

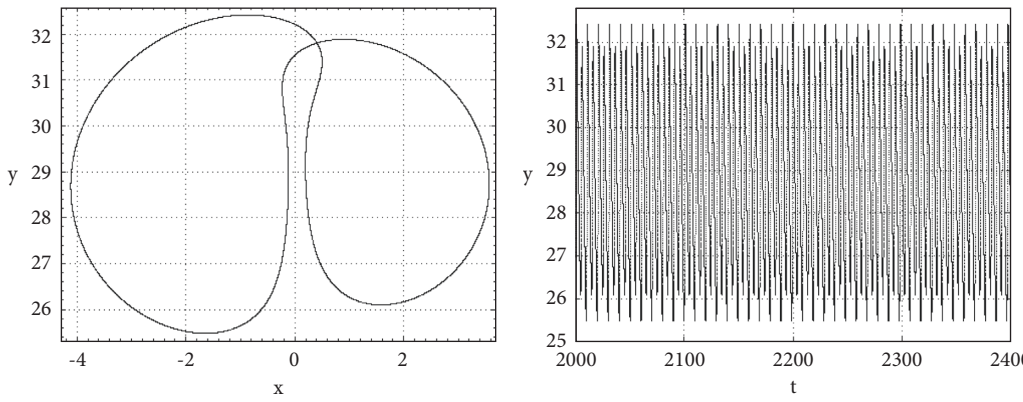

FIGURE 25: Phase portrait (a) and time series (b) of the system when the value of control parameters kf = 0.02 −0.035 and to = 0.5. The rest of parameters are x0 = 0.01; y0 = 0.01; z0 = 20; c = 30; u = 0.009; v = 0.005; beta = 0.03; $\sigma = 3.105$; (a) $T_3 = 0.001$.

7. Conclusion

In this paper, the dynamical and control of the PMSM are studied by varying the amplitude of three different loads torque: constant load torque, sinusoidal load torque, and square load torque. We highlighted the industrial situations where the amplitude of the load torque of the PMSM is varied in contrast to the frequency variation in the literature, in addition to the ON/OFF load torque not yet presented as far as our knowledge goes. We showed that PMSM exhibits periodic and chaos behavior with new shape of attractors, and chaos bursting and intermittency oscillations. These finding dynamics in these engineering applications of the PMSM need to be shared. In addition, we implement successfully the self-feedback delay controller which stabilized the PMSM from chaotic regime in the desired periodic state.

Furthermore, the electronic verifications based on the OrCAD-PSpice environment are in good agreement with numerical results obtained. Complexity and losses occurring will be investigated in a real experiment of the PMSM in future research [45, 46].

Data Availability

The data used to support the findings of this study are available from the corresponding author upon request.

Conflicts of Interest

The authors declare that they have no conflicts of interest regarding the publication of this paper.

Acknowledgments

The authors would like to thank Jeatsa kitio Gabin and Ayemtsa Gideon both of Research Unit of Automation and Applied Computer (UR-AIA), IUT-FV, University of Dschang, for their constructive discussions that help to improve the quality of the manuscript.

References

[1] S. Gao, K. T. Chau, C. Liu, D. Wu, and C. C. Chan, "Integrated energy management of plug-in electric vehicles in power grid with renewables," *IEEE Transactions on Vehicular Technology*, vol. 63, no. 7, pp. 3019–3027, 2014.

[2] A. M. Harb, "Nonlinear chaos control in a permanent magnet reluctance machine," *Chaos, Solitons & Fractals*, vol. 19, no. 5, pp. 1217–1224, 2004.

[3] R. M. Stewart, "A simple graphical method for constructing families of Nyquist diagrams," *Journal of the Aeronautical Sciences*, vol. 18, no. 11, pp. 767-768, 1951.

[4] M. S. Mahmoud and A. A. Bahnasawi, "Asymptotic stability for a class of linear discrete systems with bounded uncertainties," *IEEE Transactions on Automatic Control*, vol. 33, no. 6, pp. 572–575, 1988.

[5] F. N. Bailey, D. Panzer, and G. Gu, "Two algorithms for frequency domain design of robust control systems," *International Journal of Control*, vol. 48, no. 5, pp. 1787–1806, 1988.

[6] F. N. Bailey and C.-H. Hui, "A fast algorithm for computing parametric rational functions," *IEEE Transactions on Automatic Control*, vol. 34, no. 11, pp. 1209–1212, 1989.

[7] A. Karamancioglu, V. Dzhafarov, and C. Özemir, "Frequency response of PID-controlled linear interval systems," *Circuits, Systems, and Signal Processing*, vol. 15, no. 6, pp. 735–748, 1996.

[8] C. Hwang and J.-J. Chen, "Computation of the frequency response of interval systems," *Circuits, Systems, and Signal Processing*, vol. 15, no. 6, pp. 807–818, 1996.

[9] A. C. Bartlett, A. Tesi, and A. Vicino, "Frequency response of uncertain systems with interval plants," *IEEE Transactions on Automatic Control*, vol. 38, no. 6, pp. 929–933, 1993.

[10] Y. Kuroe and S. Hayashi, "Analysis of bifurcation in power electronic induction motor drive systems," in *Proceedings of the 20th Annual IEEE Power Electronics Specialists Conference*, IEEE, Milwaukee, WI, USA, 1989.

[11] W. Souhail, H. Khammari, and M. F. Mimouni, "Bifurcation control and complex dynamics in field-oriented control of a PMSM," *Journal of Circuits, Systems, and Computers*, vol. 28, no. 04, Article ID 1930004, 2019.

[12] X. Chen, S. Yuan, and Z. Peng, "Nonlinear vibration for PMSM used in HEV considering mechanical and magnetic

coupling effects," *Nonlinear Dynamics*, vol. 80, no. 1, pp. 541–552, 2015.

[13] B. N. Mobarakeh, F. Meibody-Tabar, and F. Sargos, "Robustness study of a model-based technique for mechanical sensorless PMSM," in *Proceedings of the 2001 IEEE 32nd Annual Power Electronics Specialists Conference*, IEEE, Vancouver, BC, Canada, 2001.

[14] Z. Li, J. B. Park, Y. H. Joo, B. Zhang, and G. Chen, "Bifurcations and chaos in a permanent-magnet synchronous motor," *IEEE Transactions on Circuits and Systems I: Fundamental Theory and Applications*, vol. 49, no. 3, pp. 383–387, 2002.

[15] A. Cheukem, A. S. K. Tsafack, S. T. Kingni, C. C. Andre, and J. R. M. Pone, "Permanent magnet synchronous motor: chaos control using single controller, synchronization and circuit implementation," *SN Applied Sciences*, vol. 2, no. 3, pp. 1–11, 2020.

[16] A. S. Kemnang Tsafack, C. Ainamon, A. Cheukem, S. T. Kingni, J. R. M. Pone, and G. Kenne, "Control of coexisting and chaotic attractors in brushless direct current motor," *Journal of Control, Automation and Electrical Systems*, vol. 32, no. 2, pp. 472–481, 2021.

[17] S. T. Kingni, A. Cheukem, P. R. N. Tuwa, A. C. Chamgoué, V.-T. Pham, and S. Jafari, "Synchronous reluctance motor with load vibration perturbation: analysis, electronic implementation and adaptive backstepping sliding mode control," *Iranian Journal of Science and Technology, Transactions of Electrical Engineering*, vol. 45, no. 2, pp. 645–654, 2021.

[18] A. S. Kemnang Tsafack, J. R. M. Pone, A. Cheukem, R. Kengne, and G. Kenne, "Coexisting attractors and bursting oscillations in IFOC of 3-phase induction motor," *The European Physical Journal—Special Topics*, vol. 229, no. 6, pp. 989–1006, 2020.

[19] A. S. K. Tsafack, J. R. M. Pone, A. Cheukem, R. Kengne, and G. Kenne, "Chaos control using self-feedback delay controller and electronic implementation in IFOC of 3-phase induction motor," *Chaos Theory and Applications*, vol. 2, no. 1, pp. 40–48, 2020.

[20] E. H. Abed, H. O. Wang, J. C. Alexander, A. M. A. Hamdan, and H.-C. Lee, "Dynamic bifurcations in a power system model exhibiting voltage collapse," *International Journal of Bifurcation and Chaos*, vol. 03, no. 05, pp. 1169–1176, 1993.

[21] C. Rajagopalan, P. W. Sauer, and M. Pai, "Analysis of voltage control systems exhibiting Hopf bifurcation," in *Proceedings of the 28th IEEE Conference on Decision and Control*, IEEE, Tampa, FL, USA, 1989.

[22] A. M. Harb and W. A. Ahmad, "Control of chaotic oscillators using nonlinear recursive backstepping controllers," *Journal of Bifurcation and Chaos*, vol. 9, no. 11, pp. 2189–2196, 1999.

[23] N. Hemati, "Strange attractors in brushless DC motors," *IEEE Transactions on Circuits and Systems I: Fundamental Theory and Applications*, vol. 41, no. 1, pp. 40–45, 1994.

[24] N. Hemati and M. C. Leu, "A complete model characterization of brushless DC motors," *IEEE Transactions on Industry Applications*, vol. 28, no. 1, pp. 172–180, 1992.

[25] H.-S. Choi, Y.-H. Park, Y. Cho, and M. Lee, "Global sliding-mode control. Improved design for a brushless DC motor," *IEEE Control Systems Magazine*, vol. 21, no. 3, pp. 27–35, 2001.

[26] B. Zhang, Y. Lu, and Z. Mao, "Bifurcations and chaos in indirect field-oriented control of induction motors," *Journal of Control Theory and Applications*, vol. 2, no. 4, pp. 353–357, 2004.

[27] N. Jabli, H. S. Khammari, M. F. Mimouni, and R. Dhifaoui, "Bifurcation and chaos phenomena appearing in induction motor under variation of PI controller parameters," *WSEAS Transactions on Systems*, vol. 9, no. 7, pp. 784–793, 2010.

[28] K. Chakrabarty and U. Kar, "State variable participation in the limit cycle of induction motor," *Pramana*, vol. 84, no. 3, pp. 423–441, 2015.

[29] N. Hemati and H. Kwatny, "Bifurcation of equilibria and chaos in permanent-magnet machines," in *Proceedings of the 32nd IEEE Conference on Decision and Control*, IEEE, San Antonio, TX, USA, 1993.

[30] T. M. Jahns, G. B. Kliman, and T. W. Neumann, "Interior permanent-magnet synchronous motors for adjustable-speed drives," *IEEE Transactions on Industry Applications*, vol. IA-22, no. 4, pp. 738–747, 1986.

[31] R. C. Hilborn, *Chaos and Nonlinear Dynamics: An Introduction for Scientists and Engineers*, Oxford University Press on Demand, Oxford, UK, 2000.

[32] S. H. Strogatz, *Nonlinear Dynamics and Chaos: With Applications to Physics, Biology, Chemistry, and Engineering*, Avalon Publishing, New York, NY, USA, 2014.

[33] H. William, S. A. Teukolsky, W. T. Vetterling, and B. P. Flannery, "Numerical recipes," *The Art of Scientific Computing*, Cambridge University Press, Cambridge, UK, 3rd edition, 2007.

[34] H. Kantz, "A robust method to estimate the maximal Lyapunov exponent of a time series," *Physics Letters A*, vol. 185, no. 1, pp. 77–87, 1994.

[35] C. Jeffries and J. Perez, "Observation of a Pomeau-Manneville intermittent route to chaos in a nonlinear oscillator," *Physical Review A*, vol. 26, no. 4, pp. 2117–2122, 1982.

[36] Y. Guan, V. Gupta, and L. K. Li, "Intermittency route to self-excited chaotic thermoacoustic oscillations," *Journal of Fluid Mechanics*, vol. 894, 2020.

[37] I. M. De la Fuente, L. Martinez, and J. Veguillas, "Intermittency route to chaos in a biochemical system," *Biosystems*, vol. 39, no. 2, pp. 87–92, 1996.

[38] A. Ngo Mouelas, T. Fonzin Fozin, R. Kengne, J. Kengne, H. B. Fotsin, and B. Z. Essimbi, "Extremely rich dynamical behaviors in a simple nonautonomous Jerk system with generalized nonlinearity: hyperchaos, intermittency, offset-boosting and multistability," *International Journal of Dynamics and Control*, vol. 8, no. 1, pp. 51–69, 2020.

[39] V. Jan, "Energy optimal control of PMSM drive for time-varying load torque," *Applied Mechanics & Materials*, vol. 710, 2014.

[40] D. Janiszewski, "Load torque estimation in sensorless PMSM drive using Unscented Kalmana Filter," in *Proceeding of the 2011 IEEE International Symposium on Industrial Electronics*, IEEE, Gdansk, Poland, 2011.

[41] D. C. Hamill, "Learning about chaotic circuits with SPICE," *IEEE Transactions on Education*, vol. 36, no. 1, pp. 28–35, 1993.

[42] G. Bianchi, N. V. Kuznetsov, G. A. Leonov, S. M. Seledzhi, M. V. Yuldashev, and R. V. Yuldashev, "Hidden oscillations in SPICE simulation of two-phase Costas loop with non-linear VCO," *IFAC-PapersOnLine*, vol. 49, no. 14, pp. 45–50, 2016.

[43] S. Vaidyanathan, P. S. Godwin Anand, A. Sambas, and S. Zhang, "A new four-dimensional nonlinear plant with double-scroll hyperchaotic oscillator and its electronic circuit realization," in *Proceedings of the 2018 International Conference on Circuits and Systems in Digital Enterprise Technology (ICCSDET)*, IEEE, Kottayam, India, 2018.

[44] C. Ainamon, V. K. Tamba, J. R. M. Pone, and S. T. Kingni, "Analysis, circuit realization and controls of an autonomous Morse jerk oscillator," *SeMA Journal*, vol. 78, pp. 1–19, 2021.
[45] J. Xu, B. Zhang, X. Kuang, H. Guo, and S. Guo, "Influence analysis of slot parameters and high torque density optimisation for dual redundant permanent magnet motor in aerospace application," *IET Electric Power Applications*, vol. 14, no. 7, pp. 1263–1273, 2020.
[46] K. Chau, J. H. Chen, C. C. Chan, J. K. H. Pong, and D. T. W. Cha, "Chaotic behavior in a simple DC drive," in *Proceedings of Second International Conference on Power Electronics and Drive Systems*, IEEE, Singapore, 1997.